1973

Investigation of external burning assisted projectile.

Naber, Michael Edmund.

Monterey, California. Naval Postgraduate School

INVESTIGATION OF EXTERNAL BURNING ASSISTED PROJECTILE

Michael Edmund Naber

NAVAL POSTGRADUATE SCHOOL
Monterey, California

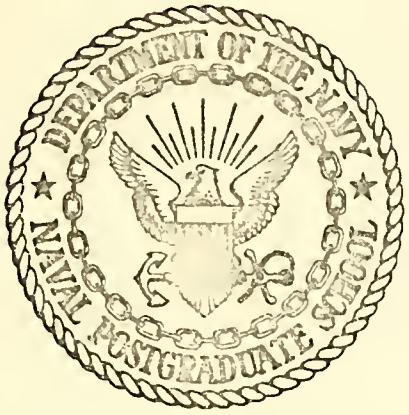

THESIS

INVESTIGATION OF EXTERNAL

BURNING ASSISTED PROJECTILE

by

Michael Edmund Naber

Thesis Advisor: A. E. Fuhs

September 1973

Approved for public release; distribution unlimited.

Investigation of External Burning Assisted Projectile

by

Michael Edmund Naber
Lieutenant, United States Navy
B.S., United States Naval Academy, 1966

Submitted in partial fulfillment of the
requirements for the degree of

MASTER OF SCIENCE IN AERONAUTICAL ENGINEERING

from the

NAVAL POSTGRADUATE SCHOOL
September 1973

ABSTRACT

External burning reduces the base drag of a supersonic projectile by increasing the base pressure. Drag reduction is of interest due to the increase in range, decreased time of flight and/or increased impact velocity. Theoretically, the Crocco-Lees analytical model for base flow is reviewed for axisymmetric flow without heat addition and for planar flow with heat addition. A free jet wind facility has been constructed for simulation of a projectile with heat addition. Heat addition is found to give base thrust and, therefore, provides a method for increasing the performance of a gun system.

TABLE OF CONTENTS

LIST OF TABLES

LIST OF ILLUSTRATIONS

LIST OF SYMBOLS

A	Area
A_h, A_c	Areas of heat addition and adiabatic free stream, respectively
a	Speed of sound
b	Capture height of heat addition zone
D	Drag
F	$(f/\kappa^2) - 1.0$
f	Parameter appearing in mean temperature–velocity
g	Function defined by equations 29–32
I	Momentum flux
k	Mixing rate coefficient
l	Length of combustion zone
M	Mach number
m	Mass flux
P	Pressure
q	Heat release per unit volume per unit time
R	Gas constant
r	Radius
T	Temperature
U	Velocity
W	Ratio of velocity to stagnation velocity
X, Y	Coordinates
X_i, Y_i	Values of X and Y at initiation of combustion

β	$\sqrt{m^2-1}$
γ	Ratio of specific heats
δ	Boundary layer thickness
δ^*	Displacement thickness
δ^{**}	Momentum thickness
$\Delta( )$	An incremental change in ( )
$\Delta V/V$	Fractional change in volume at constant pressure
Δh_f	Heat release per unit mass of fuel
η	Heating parameter
θ	Local angle
κ	U_l/U_e, W_l/W_e
μ	Coefficient of viscosity
ν	Prandtl-Meyer function
ρ	Density
ϕ	Perturbation velocity potential

Subscripts

B	Denotes base
b	Boundary layer on forebody just ahead of base
e	Edge of viscous layer
i	Incompressible
t	Stagnation
∞	Free stream

ACKNOWLEDGEMENT

The author wishes to express his appreciation to Professor A. E. Fuhs for his patience and guidance. The author would also like to express his thanks to Commander W. J. N. Smithey, who is working on the same subject, for making things understandable and to Messrs H. Connors and J. Moulton for their technical assistance. Finally, the author wishes to acknowledge his thanks to Mr. Dominic Monetta and Dr. Alan Roberts of Gun System Engineering, Naval Ordnance Station, Indian Head, Maryland, for their support.

I. INTRODUCTION

For a blunt based axisymmetric body in supersonic flight, most of the drag is produced in the base region. The mechanics that produce this drag are known in general, and several analytical approaches are available to predict the pressure drop that creates the drag. Conceptually, the base drag can be localized and is directly related to the ratio of base pressure to free stream pressure; suitable methods are needed to raise this pressure ratio to 1 or hopefully in excess of 1.

To date external burning seems to have the greatest potential for base drag alleviation through heat addition. Heat addition in the form of a torus around the body in the inviscid region in close proximity to the base will create compression waves that will impinge upon the base region. Depending upon the position of the heat addition region these compression waves will interact with the boundary layer close to the base and/or the viscous shear layer training from the base expansion corner.

Normally when a supersonic flow passes a corner, it will turn through an expansion fan increasing its speed with a corresponding loss of pressure. With the addition of compression waves, a further turning of the flow in the direction of the axis can be expected but without a change

in Mach number or a further decrease in pressure. For the flow field around the projectile to be balanced, the pressure within the region entrapped by the viscous shear layer would have to increase.

This thesis has two areas of interest. First, a review of the base flow is presented based on the analytical approach of Crocco-Lees [Ref. 1] as the guide. The second is an experiment to determine the influence of heat addition on the base pressure and to optimize empirically the length and position of the heat addition zone.

II. DISCUSSION OF THEORY

In 1952 Crocco and Lees [Ref. 1] were the first to formulate an acceptable theoretical model for flow problems treating the interaction between a viscous shear layer close to a body and the outer nearly isentropic flow. One major contribution of the model was the introduction of the concept of mixing of the transport of momentum from the outer stream to the inner shear layer.

With this model they analyzed two-dimensional planar wake flow behind blunt based bodies. Taking the mixing rate proportional to the mass flux of the external isentropic flow, the equations of motion were reduced to a single nonlinear equation. This differential equation has a singularity or critical point known as a saddle point. One and only one integral curve can pass through the singularity with all other adjacent curves blowing up to positive or negative values. See Figure 1. When related to the flow, the singular point acts, on the average, similar to the throat of a nozzle and uniquely determines the entire flow and the base pressure.

In the derivation of the differential equation several functional relationships are used or introduced. One that was introduced which is of more than passing interest is $F(\kappa)$, where

$$F = \frac{f}{K} - 1 \qquad (1)$$

$$\kappa = \frac{W}{W_e} = \frac{\delta - \delta^* - \delta^{**}}{\delta - \delta^*} \tag{2}$$

and

$$F = \frac{(\delta - \delta^* - \delta^{**})\,\delta}{(\delta - \delta^*)^2} \tag{3}$$

This relationship between F and κ is a general function for all types of incompressible flow and, therefore, with suitable transformations, for many types of compressible flows. A curve (see Figure 2) can be drawn for turbulent flows with $\kappa = 0.72$ and $F > 1.5$ corresponding to half of a jet; and as $\kappa \Rightarrow 1.0$ and $F \Rightarrow 0.0$, the curve corresponds to far wake flows. Strahle [Ref. 2] added to the interpolation of the graph by noting that the point at $\eta = 0.89$ corresponds to a flat plate and that $F = 1.5$ corresponds to the rear stagnation point of the recirculation bubble.

During the period that Crocco and Lees wrote their paper on the mixing theory, Davis [Ref. 3], a graduate student working with Lees, expanded the Crocco-Lees simplified theory to the axisymmetric case. This transformation will now be discussed; refer to Figure 3 for geometry of the flow.

The mass flux is

$$\bar{m} = 2\pi \int_0^\delta \rho U r\, dr \tag{4}$$

and the momentum flux is

$$I = 2\pi \int_0^\delta \rho U^2 r\, dr \tag{5}$$

for the internal stream. The rate at which mass is transported to the internal flow is

$$\frac{dm}{dx} = 2\pi\rho U\delta\left(\frac{d\delta}{dx} - \Theta\right) \tag{6}$$

The momentum balance in the absence of wall shear stress becomes

$$dI = U_e\,dm - \pi\delta^2\,dP \tag{7}$$

Since dm/dx is assumed to be proportional to the mass flux at the edge of the boundary layer, k, a nondimensional mixing coefficient that must be specified, is introduced

$$\frac{dm}{dx} = 2\pi\delta\rho U k \tag{8}$$

A mean velocity, density and temperature are defined

$$U_1 = \frac{I}{\bar{m}} \tag{9}$$

$$\bar{m} = \pi\delta^2\rho_1 U_1 \tag{10}$$

$$T_1 = \frac{P}{\rho_1 R} \tag{11}$$

A velocity ratio can be defined as

$$K = \frac{U_1}{U_e} = \frac{I}{\bar{m}\,U_e} \tag{12}$$

which is important because the ratio becomes the independent variable for the Crocco-Lees universal function. The displacement and momentum thickness now needs to be redefined

$$\delta^{*2} = 2\int_0^{\delta} \left(1 - \frac{\rho U}{\rho_e U_e}\right) r\,dr = \delta^2 - \frac{\bar{m}}{\pi \rho_e U_e} \tag{13}$$

$$\delta^{**} = 2\int_0^{\delta} \frac{\rho U}{\rho_e U_e}\left(1 - \frac{U}{U_e}\right) r\,dr = \delta^2 - \delta^{*2} - \frac{I}{\pi \rho_e U_e} \tag{14}$$

Substituting into

$$K = \frac{I}{\bar{m} U_e} = \frac{\delta^2 - \delta^{*2} - \delta^{**2}}{\delta^2 - \delta^{*2}} = \frac{\delta_i^2 - \delta_i^{*2} - \delta_i^{**2}}{\delta_i^2 - \delta_i^{*2}} \tag{15}$$

Stewartsons' [Ref. 4] transformation is used to obtain equivalent incompressible viscous flows. By application of the transformation, it can be shown that incompressible flow is identical with the addition of the subscript i to all symbols as shown above. For one-dimensional flow, the relationship between the total to static temperature is

$$\frac{T_i}{T_s} = 1 - \frac{\gamma - 1}{2} W_e^2 K^2 \tag{16}$$

with

$$W_e = \frac{U_e}{a_s} \tag{17}$$

For this flow a similar equation would be

$$\frac{T}{T_s} = f - \frac{\gamma - 1}{2} W_e \tag{18}$$

with

$$f = K \frac{\delta^2}{\delta^2 - \delta^{*2}} \tag{19}$$

A more convenient relation is defined as

$$F = \frac{f}{K^2} - 1 \tag{20}$$

With considerable manipulation and substitution dF/dW_e can be solved for

$$\frac{dF}{dW_e} = \frac{\left(\frac{\gamma-1}{2} W_e^2 - 1\right)\left(1 - \frac{\gamma-1}{2} W_e^2\right) + F\left[\gamma W_e - \frac{KF}{1-K} + \frac{\theta_e}{K}\frac{\left(1 - \frac{\gamma-1}{2} W_e\right)}{(1-K)}\right]}{W_e\left(1 - \frac{\gamma-1}{2} W_e^2\right)\left\{\left[\frac{\theta_e}{K}\frac{\left(1 - \frac{\gamma-1}{2} W_e^2\right)}{K(1-K)} - \frac{F}{K(1-K)}\right]\frac{dK}{dF} - 1\right\}} \tag{21}$$

This nonlinear differential equation is identical to equation (2-30) of the Crocco-Lees paper. To solve this equation for axisymmetric flow, a guess must be made for θ_e and W_e because they are not simply related by the Prandtl-Meyer function as in the planar case. This requires the use of the method of characteristics [Ref. 5] starting at the base with several iterations necessary to find the correct values instead of starting at the critical point in the planar case. Davis also used the planar relationship for F-K from the Crocco-Lees paper.

In 1964, for a Ph.D. thesis, de Kransinski [Ref. 6] re-examined the base flow problem for the axisymmetric case including the Crocco-Lees analytical model and Davis'

extension. Extensive experimentation was carried out, and his empirical data were able to confirm several important aspects of the Crocco–Lees theory.

His data showed that the transport of momentum or mixing played a dominant role in the determination of the separated flow field and the base pressure. As the boundary/shear layer undergoes transition from laminar to turbulent flow, with the corresponding increase in the transport of momentum, the base pressure decreases; see Figure 4. The evidence also indicated that the throat region, which corresponds to the saddle point of the differential equation, is the pivotal point that controls the flow field and therefore the base pressure.

Since it is well established how the major proportion of drag is created on a blunt based body, techniques to manipulate or alleviate the base drag are being studied. Previous methods, both analytical and experimental, tended to work with mass or heat addition at the base of the body within the shear layer or the recirculation bubble. They tended to give limited base pressure increases and to have low efficiency.

An approach that shows a great deal of promise is Strahle's method [Ref. 2]. On reviewing previous work, he noted one experiment that added heat in the inviscid region and gave a large pressure increase. Using this

experiment as a basis, he developed a model for heat addition adjacent to a two-dimensional planar, supersonic, turbulent, base flow.

The method chosen to treat the base flow is the mixing theory of Crocco-Lees. He felt that although it did not answer all questions about base flow, it was adequate for the prediction of the base pressure. The differential equation will still have a critical point that uniquely defines the flow, but its position and influence will be altered by combustion.

In treating the heat addition region, Strahle used two methods for formulation: the linear heat addition theory, which contradicts the assumptions beyond small values of heat release; and the one-dimensional heat addition model matched to a two-dimensional planar flow.

Using the linear theory, the perturbation velocity potential equation describing the flow is

$$-\beta_B^2 \phi_{xx} + \phi_{yy} = f \tag{22}$$

with

$$f \equiv (\gamma - 1) q / \rho_B a_B^2 \tag{23}$$

The quantity f is non-zero for positive X and Y values. The geometry is illustrated in Figure 5. Upon integrating along the Y = 0 line

$$\theta_x(X,0) = \frac{1}{\beta_B^2} \int_0^X f\left[X', \left(\frac{X - X'}{\beta_B}\right)\right] dX \tag{24}$$

Since the initial turning angle is unknown, Bernoulli's equation is used

$$\frac{dP}{\rho U^2} = -\frac{dU}{U} = \frac{d\theta}{\sqrt{M^2-1}} - \frac{d(\phi_x)}{U} = \frac{d(M^2)}{2M^2\left(1-\frac{\gamma-1}{2}M^2\right)} \tag{25}$$

Upon rewriting and integrating

$$\theta - \theta_b = \nu(M_b) - \nu(M) + \frac{\beta_b}{U_B}\phi_x \tag{26}$$

which consists of the Prandtl-Meyer terms and the heat addition term.

Equation (26) must now be evaluated through several regions to solve the differential equation:

$$\theta - \theta_b = \nu(M_b) - \nu(M) - \eta\, g(x) \tag{27}$$

with

$$\eta = \frac{(\gamma-1)\,\Delta h_f}{\beta_B\, a_B^2\, \mu\, l} \tag{28}$$

where for

$$g(x) = 0 \qquad X < X_1,\ X > X_4 \tag{29}$$

$$g(x) = X - X_i - \beta_B Y_i \qquad X_1 \le X < X_2 \tag{30}$$

$$g(x) = \beta_B b \qquad X_2 \le X < X_3 \tag{31}$$

$$g(x) = \beta_B (Y_i + b - X + X_i + l) \qquad X_3 \le X \le X_4 \tag{32}$$

and

$$X_1 = X_i + \beta_B Y_i \tag{33}$$

$$X_2 = X_i + \beta_B (Y_i + b) \tag{34}$$

$$X_3 = X_i + l + \beta_B Y_i \tag{35}$$

$$X_4 = X_i + l + \beta_B (Y_i + b) \tag{36}$$

Now for correlation, the one-dimensional approach will be used with a small angle assumption. See Figure 6. Using the one-dimensional Prandtl-Meyer relationship

$$\Theta = \Theta_b + \nu(M_b) - \nu(M) \tag{37}$$

and the one-dimensional flow relationship

$$\frac{1}{A_e}\frac{dA_e}{dx} = \frac{1 - M_e^2}{\gamma M_e^2}\,\frac{1}{P_e}\,\frac{dP_e}{dx} \tag{38}$$

and combining

$$\Theta - \Theta_b = \nu(M_b) - \nu(M) - \frac{A_e}{P_e}\,\frac{(1 - M_e^2)}{\gamma M_e^2}\,\frac{dP_e}{dx} - \frac{dA_h}{dx} \tag{39}$$

Since dP_e/dx is small, for large heat addition the last term dominates the pressure gradient term. Thus, if $\eta g(x)$ is identified with dA_h/dx, the analogy is achieved, where

$$\frac{dA_h}{dx} = \frac{b}{\ell}\,\frac{\Delta V}{V} \tag{40}$$

so that

$$\frac{\Delta V}{V} = \frac{(\gamma - 1)}{\mu\, a_\infty^2}\,\Delta h_f \tag{41}$$

and

$$\eta = \frac{\Delta V}{V}\,\frac{1}{\ell\,\beta_B} \tag{42}$$

Using η as defined in equation (42) through the regions previously defined, several wake solutions were made that reasonably accounted for the effects of combustion and mass addition.

From the analysis Strahle concluded that external burning adjacent to the viscous near wake will increase the base pressure and can produce base thrust. The amount of increase in the base pressure for a given Mach number is dependent upon only the heat addition length and intensity. He also noted that base pressure rise was insensitive to the state of the boundary layer, the form of the trailing edge and distance from the centerline of the heat addition zone.

Before looking at axisymmetric heat addition, a general understanding of the changes to be expected between planar and axisymmetric results can be accomplished through a simple analysis pointed out by Fuhs [Ref. 7].

The change in base drag is $\Delta D = \Delta P_B A_B$. Consider the area term for both cases. See Figure 7. If heat is released along r_2 in each case with a constant heat release per unit length, a ratio of areas influenced can be made

$$\frac{\text{Axisymmetric}}{\text{Planar}} = \frac{\pi r_1^2}{\lambda \pi r_1 r_2} = \frac{r_1}{\lambda r_2} \qquad (43)$$

This indicates the axisymmetric case has less area to be influenced. For ΔP_b flow through an annular heat addition region was looked at using the method of characteristics with the following results:

1. With axial symmetry the compression waves merge sooner.
2. The increase of pressure with decreasing radius is very small until the axis is approached.

III. DESCRIPTION OF APPARATUS AND EXPERIMENTS

For the design and fabrication of a wind tunnel model to simulate heat addition on a projectile, certain design parameters were needed. Those selected were for a 5-inch projectile in flight at approximately 23,000 feet with a Mach number equal to 2.0. For a turbulent boundary layer on the projectile, the Reynolds number as the boundary layer reaches the base is 1.5×10^6, and using the 1/7 power law for the displacement thickness, the ratio of the displacement thickness to the radius is $\delta^*/r = 0.0164$. With the above information, scale, dimensions, pressure and density requirements can be ascertained.

Initially, for a system check, the data desired were the ratio of base pressure to free stream pressure P_b/P_∞ under conditions without heat addition. Heat addition simulated by compression waves was then introduced to study the effect on the base pressure ratio.

Figure 8 shows the general arrangement of the equipment employed in this series of experiments. Air, which is taken from a reservoir at approximately 300 psig, is controlled by a gate valve and a pressure regulating valve. A gage is mounted on the pressure regulator to give the pressure of the regulated air. The flow then is turned 90° by an elbow. A metal spacing ring (part 3, Figure 8b)

is mounted on the elbow and provides a conduit for the plastic tubes connected to pressure taps (part 13, Figure 8b). Mounted above the spacer is a 3-foot section of pipe used for stabilizing the air flow. Through the center of the flow straightener section is the cylinder extension, supported at the lower and upper ends by flow straighteners (part 12 in Figure 8b). Next is the coaxial nozzle with the cylinder through it shown in Figure 9. Around the nozzle as a safety precaution, in the event of a failure during a run, is a steel casing. The steel casing is used also as a support for mounting of the pitot tube. The cylinder has six pressure taps, four on the base and two on the side for base and upstream pressure measurements. Tubes, connected to the taps, proceed down through the cylinder and the cylinder extension. The tubes then go through a cap-tube assembly and out the side of the spacer. To the right of the free jet, as shown in Figure 8a, is a 6-tube mercury manometer to which the tubes connect. In the background is a mirror that is part of the schlieren used for flow visualization and pictures. In the foreground are some of the nozzles and spacers.

In the initial design stage of the axisymmetric coaxial nozzle a special problem developed; the shape and location of the sonic line was not known. Once the position of the sonic line is known, the method of characteristics can be used to determine nozzle wall contour.

Theory had not been developed to determine the sonic line in a coaxial nozzle. A method was developed that solved this problem [Ref. 8]. Uniform flow, which corresponds to the condition of zero heat addition, was used as the base-line configuration. Heat addition in the form of compression waves could then be introduced through appropriate nozzle contour changes.

The heat addition that could be obtained from fuel rich solid propellant was simulated by suitable nozzle wall contours. The one chosen was ARC-163. With its heat release of 7200 to BTU/lbm and using a mass flow rate of 0.6 lbm/sec and a ΔT equal to 3060°F, stoichiometric burning was approximated.

When the flow was related to the available heat, the results indicated a 4.5° turn of the flow towards the axis. The turn was introduced in 1.5° increments along a streamline initially at 1.34 radii from the centerline; spacing of the turn increments fits the mesh of the method of characteristics. Three lengths of the heat addition zone, nondimensionalized by the radius, W/r, were used. For the two smaller values of W/r, the flow is turned parallel to the axis in increments of 1.5°, thereby reestablishing uniform flow. The longest heat addition zone terminates abruptly due to the end of the nozzle. The heat addition lengths are therefore measured from initial full compression to the ending of full compression.

The initial full compression and, hence, the upstream end of the simulated heat addition zone starts at the same place for each nozzle. Five axial positions of initial full compression, all nondimensionalized by radius, P/r, were investigated. P is the distance from corner of the base to the point on the cylinder (projectile) where initial full compression is attained. The positioning downstream was done by the introduction of spacers between the flow straightener section and the nozzle; see part 6, Figure 8b.

After the free jet facilities were altered and the equipment assembled, numerous problems developed, many of which were time consuming.

The forces due to a Mach 2 jet flowing from a nozzle exit area of approximately 10 square inches were quite considerable. The facilities had to be altered twice to ensure an unobstructed and reinforced venting system. The noise and vibrations generated were also considerable. This caused suspension of one of the two methods of flow visualization intended – holography. Using a continuous wave laser in such an environment did not seem feasible, and a Q–switch laser was not available.

Initially the pictures taken using schlieren were of poor quality, having numerous horizontal lines, although the flow visualization was good. It was finally determined that the A/C source of the mercury light was causing the lines when used in conjunction with a focal plane–shutter

camera. The frequency of the light modulation was 120 Hz. A slower shutter speed was used to decrease the number of lines. A filtering lens was needed then to reduce the light because of the high speed sensitive nature of the film; it had a tendency to become overexposed.

The initial runs for calibration and system check out used a nozzle that was intended to produce a uniform M = 2.0 flow. It was found that the pressure required was higher than expected, and schlieren pictures showed Mach lines of varying angles indicating a nonuniform flow. It was felt that the nonuniformity of the flow was caused by a possible canting of the sonic line in the throat of the nozzle due to variable total pressure entering the nozzle from the flow straightener section. The flow straightener section was initially made with two sizes of tubes in a uniform pattern around the extension of the centerline cylinder such that the tube bundle was force fitted into the pipe. The spaces between the tubes gave rise to six air passages of varying shapes. This support and rigidity to the center cylinder extension was felt to be needed for future experiments involving a spinning cylinder. Upon checking the flow from the straightener section with a total pressure probe, large variations of total pressure were noted. To correct the nonuniform pressure profile, all but a 2-inch section near the lower end was removed, and a round block (part 5b, Figure 8b) was

fitted near the top with a uniform pattern of holes. All holes had identical diameter. The ratio of the length of holes to the diameter was 10. When operated again, the pressure to obtain an approximately M = 2 flow was decreased by 21% to 110 psig.

It was decided also to check for constant Mach number at the exit of the nozzle. A 21° half angle wedge was placed in the flow. The wedge leading edge was oriented parallel to the schlieren light beam and was moved across the nozzle exit in uniform steps.

Schlieren photographs were taken of the shock waves produced. At 110 psig the average Mach number was 2.09 $\pm$ 2.5%.

Although the Mach number was nearly uniform, the flow field still had compression waves and expansion fans. The appearance of extraneous compression and expansion waves was attributed to a sonic line displaced from the calculated position. Upon reexamining the nozzle design, it was decided that radius of curvature of the throat was too large and probably not anchoring the sonic line. To solve this problem, a throat with a sharp corner was used. This new nozzle produced a flow field that looked uniform. The new design was found also to be helpful when designing nozzles for simulated heat addition. The longer length of uniform flow which was obtained with the new nozzle could be used to make longer heat addition zones.

The method of measuring the pressure changed from the use of a scanner value and a single pressure gage to a six tube mercury manometer. Average run times of 40 seconds, 45 minutes pump up time between runs, and large fluctuations in pressure and vibrations produced dictated the change. Use of electronic equipment was considered and discarded due to the potential for failure in a high noise and vibrational environment.

Another problem developed when the first compression nozzle was used. The nozzles are made from epoxy using wax molds for ease and simplicity of manufacturing. The amount of resin (the polymerizing agent) used is limited because of the use of wax molds. The more resin used, the more heat generated during polymerization which increases the possibility of the mold deforming. A lesser amount of resin decreases the strength of the epoxy. After using the nozzle for several runs, the air in the tank was bled down through the nozzle. Because of the low temperature created by the large pressure drop and the long duration of the run, the nozzle became brittle and broke.

All runs were made with a pressure reading on the gage of 103 psig. This was determined by making runs at stagnation pressures that gave Mach lines close to 30 degrees; the Mach lines originated from the edge of the nozzle exit plane. Readings from the pressure taps on the side of the

cylinder were taken. A stagnation pressure of 103 psig yields atmospheric pressure on the cylinder immediately upstream of the base corner. Runs were made to verify pressures, and the Mach lines were checked for the correct angle.

IV. DISCUSSION OF RESULTS

The data obtained in the series of experiments are shown in Table I. Half of the data and the figures showing the flow fields represent the work of Lieutenant Junior Grade Gary Caswell who was also working on the free jet for his thesis. This was due to the numerous problems that developed and the time frame alloted.

The results from both types of uniform flow nozzles, shown on Figure 10, compare very favorably with the data compiled by Przirembel and Page [Ref. 9]. The nonuniformity of the flow in the contoured throat nozzle seemed to have little effect on the base pressure.

Figures 11–25 show the pictures of the flow for three W/r values through five values of P/r with drawings below each photograph representing the location and extent of heat addition. The double cross hatched areas indicate a phenomenon taking place that was not expected. In the flow fields are unexpected compression waves impinging on the recirculation region (most notably so in the pictures for W/r = 4.34). The compression waves are a reflection of the initial compression waves from the nozzle wall. Figures 26–28 show the results of analysis concerning the reflected waves for different W/r.

The reflected compression waves represent a departure from the assumption of uniform heat addition. For

W/r = 4.34, the heat addition rate is nearly doubled at the end of the zone; see Figure 29. For the shorter W/r, an extra heat addition zone is added further downstream; see Figures 30 and 31.

Although the reflected compression waves were present in all runs, it is assumed that they affected only those data points circled in Figure 10. This assumption is based on where the reflected compression waves reflect back into the flow around the cylinder. If they impinge on the cylinder or the viscous shear layer where the flow entrapped has a Mach number less than 1.0, the base pressure would be affected. When the flow behind the base of the cylinder is equal to or greater than a Mach number of 1.0, the effect of the reflected compression cannot be transmitted to the base flow. Figures 29–31 can be used to determine when the reflected compression waves will affect the base pressure. For a particular W/r, pick a P/r on the lower graph. Go across until the sonic line is hit. A line extended vertically will have on its left that part of the heat addition affecting the base pressure.

Figure 10 has P_b/P_∞ versus P/r for three W/r. All but one point shows an improvement with heat addition. Several points for P_b/P_∞ are greater than 1.0 indicating the development of base thrust.

An interesting point for speculation is the assumption that if the point of sonic flow is approximately 3 to 4

radii downstream of the base (no exact measurements were made), a trend can be found from the curves. As the downstream end of the heat addition zone approaches the sonic point, P_b/P_∞ increases. P_b/P_∞ then starts to decrease as the heat addition zone goes past. The longer heat addition zones give larger peak values of P_b/P_∞ when the end of the zone is at the sonic point.

V. CONCLUSIONS AND RECOMMENDATIONS

The following conclusions, and recommendations where appropriate, are derived from the data and photographs.

1. Heat addition not only will reduce drag but also can produce base thrust under the right conditions.
2. Heat addition has a limited effect when part or all of the heat addition zone is added upstream of the base or downstream of the sonic point in the base flow. In conjunction with this an investigation should be made starting the full compression zone at the base lip and extending the zone downstream in steps to determine the optimal length. A measurement to determine the position of the sonic point would help.
3. Combustion in an actual case may not occur in a manner yielding a pressure distribution similar to that used in this experiment; hence, empirical data on combustion generated pressure distributions would provide a basis for more accurate simulation of heat addition.
4. The general manufacturing process of nozzles should be reviewed with the intent of having nozzles that are built closer to the desired specifications and have greater strength.

TABLE I. Data Matrix

The numerical values are for P_b/P_∞.

P/r \ W/r	0.72	1.84	4.34
-2.23	0.703	0.6	1.145
-0.95	0.685	0.858	1.258
-0.5	0.759	0.96	1.20
0.0	0.893	1.055	1.14
0.5	0.993	1.074	1.085

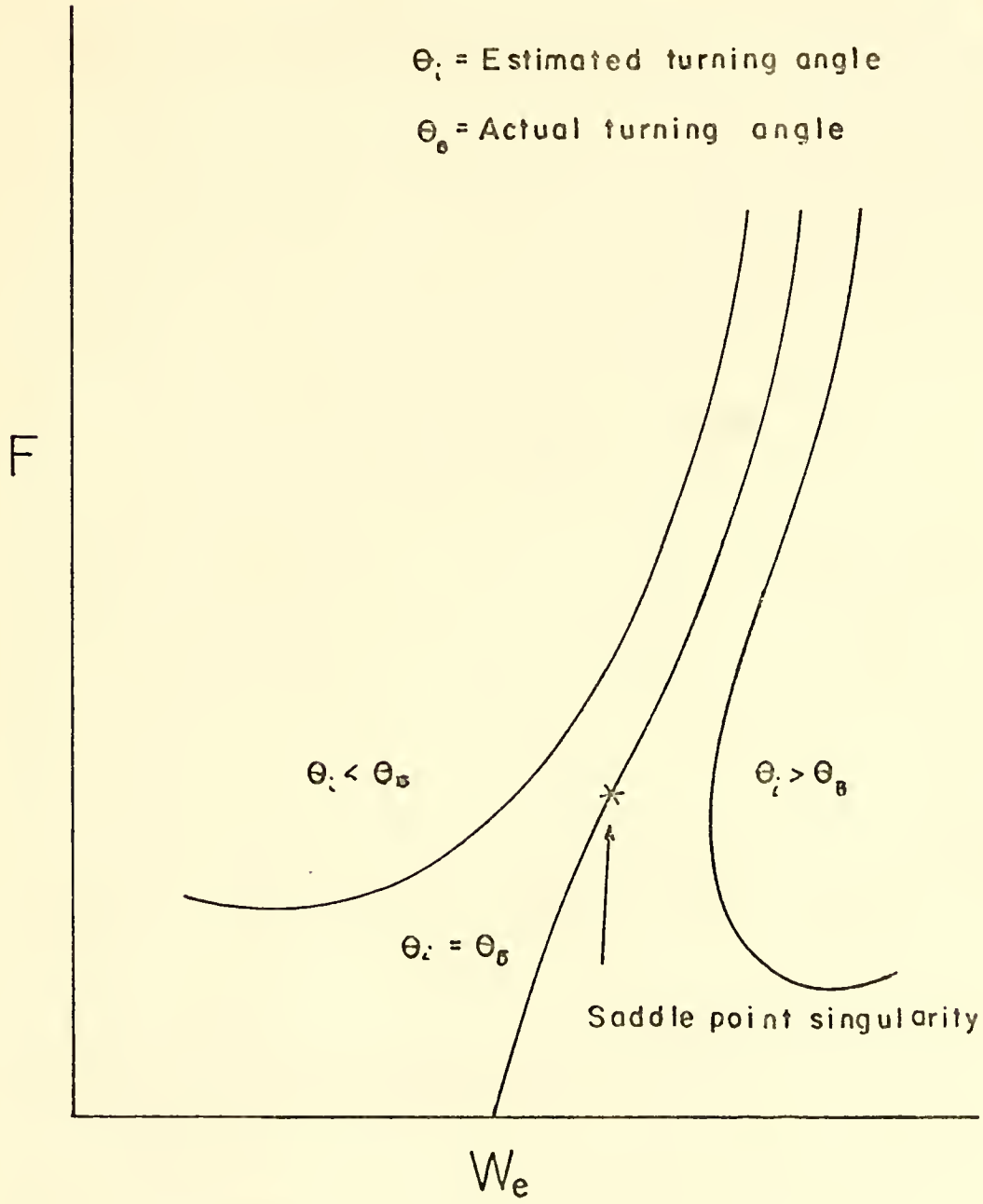

Figure 1. Significance of Critical Point.

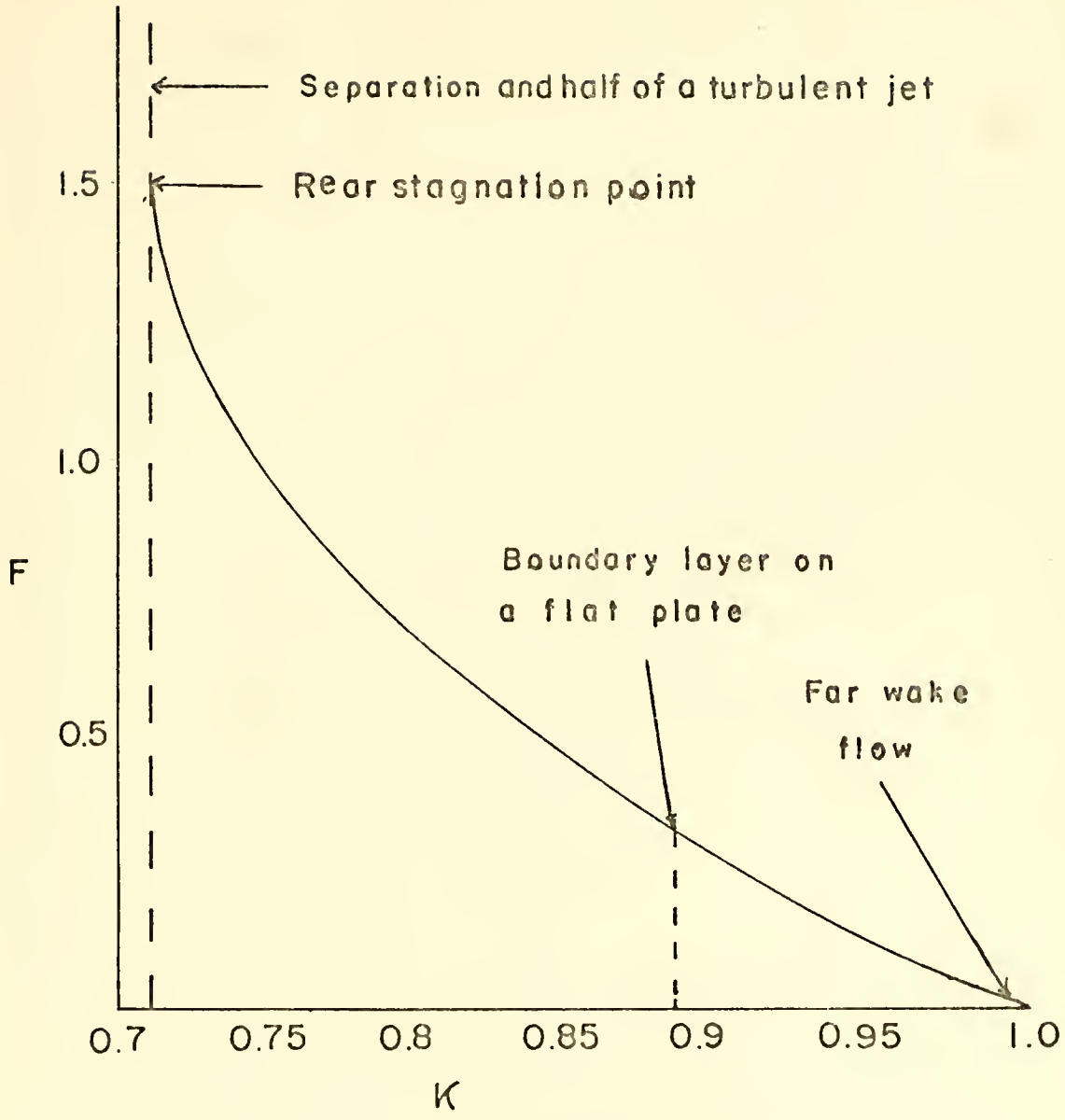

Figure 2. F–κ Curve for Turbulent Flow.

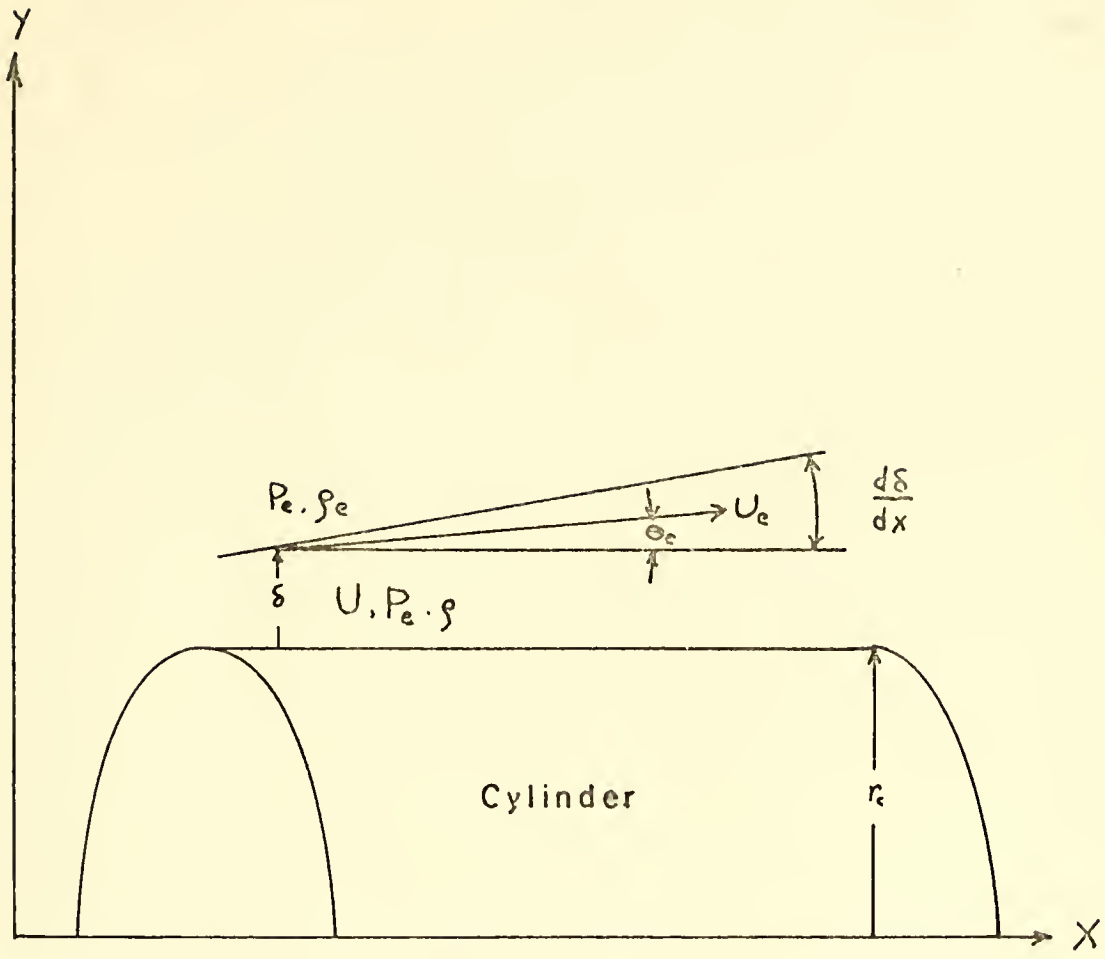

Figure 3. The Two Distinct Flow Regions; Inviscid for $r > \delta + r_c$ and Viscous for $r_c < r < r_c + \delta$.

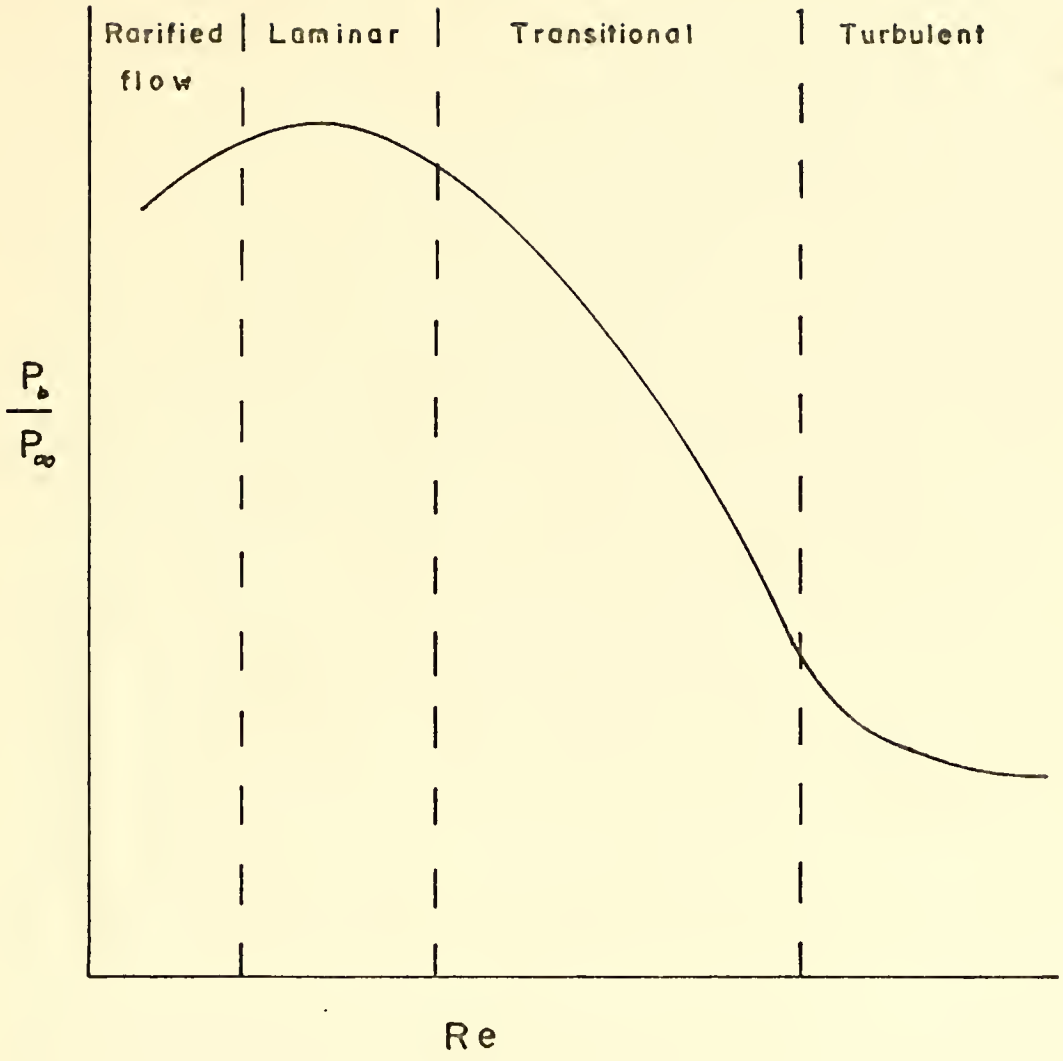

Figure 4. Base Pressure Ratio as a Function of the Reynolds Number for Constant Mach Number.

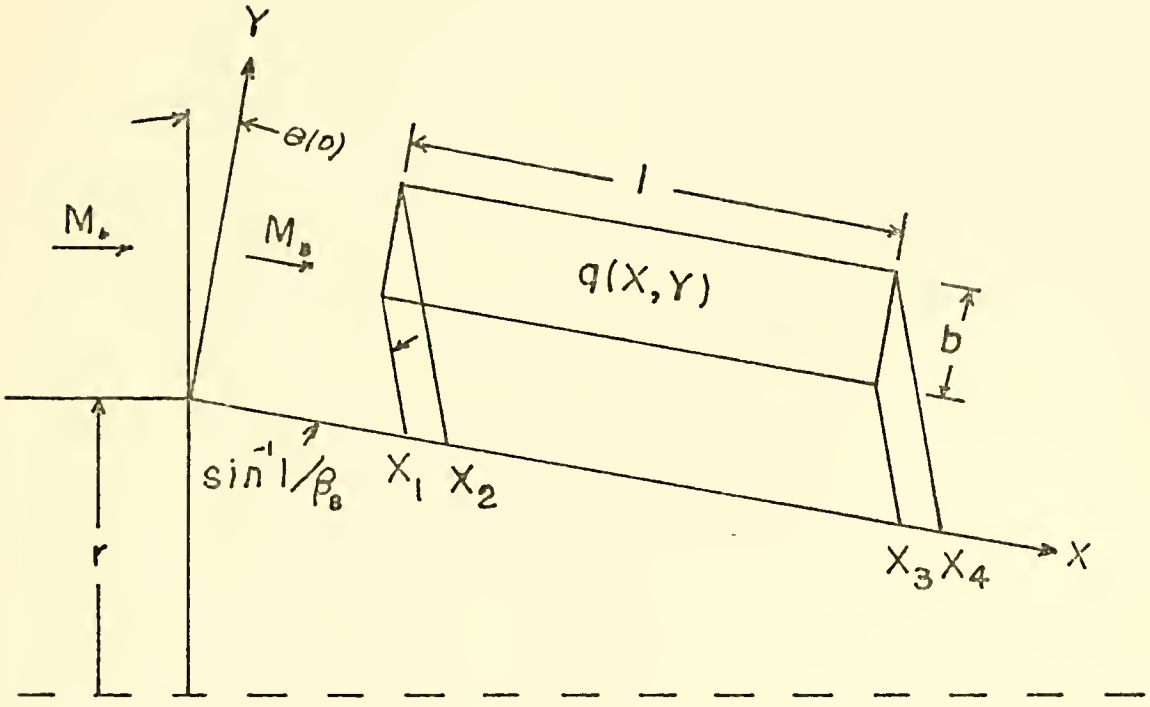

Figure 5. Linear Theory Approach to Heat Addition.

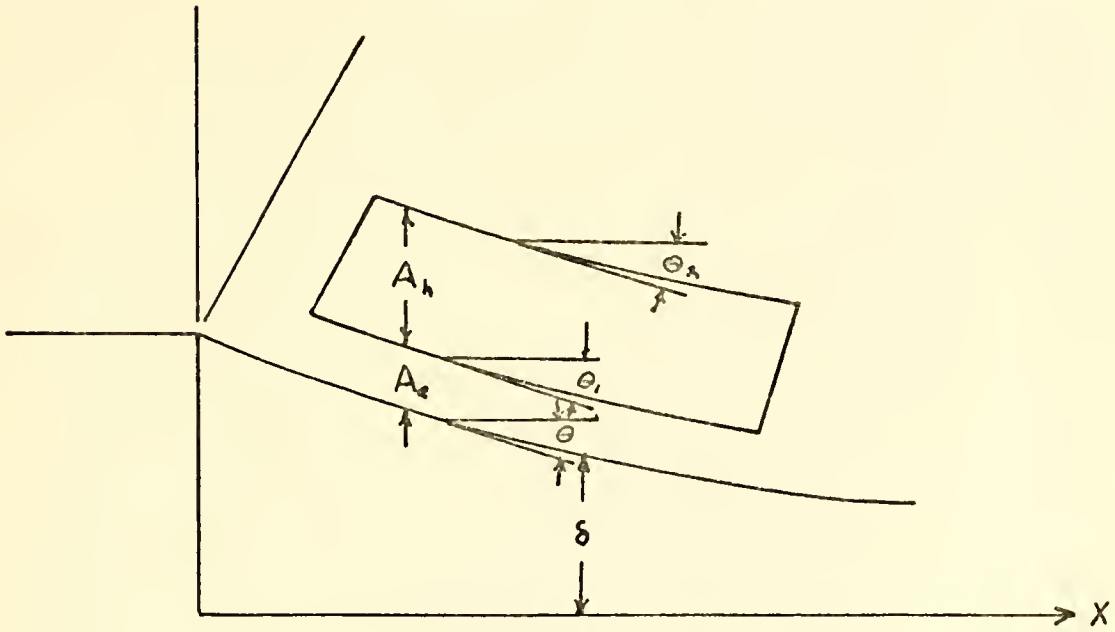

Figure 6. One-Dimensional Approach to Heat Addition.

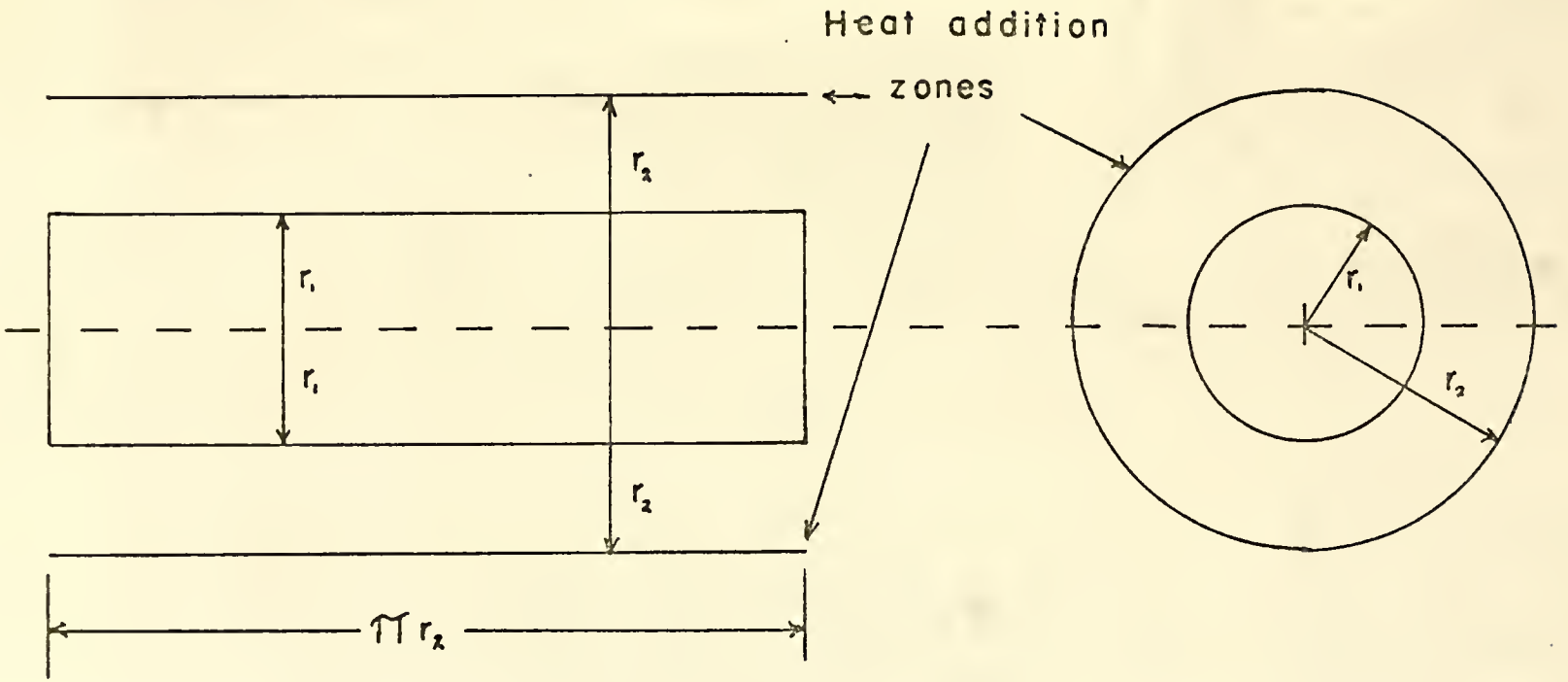

Figure 7. Comparison of Base Area for Planar and Axisymmetric Geometry.

a) Photograph
Figure 8. Free Jet Wind Tunnel.

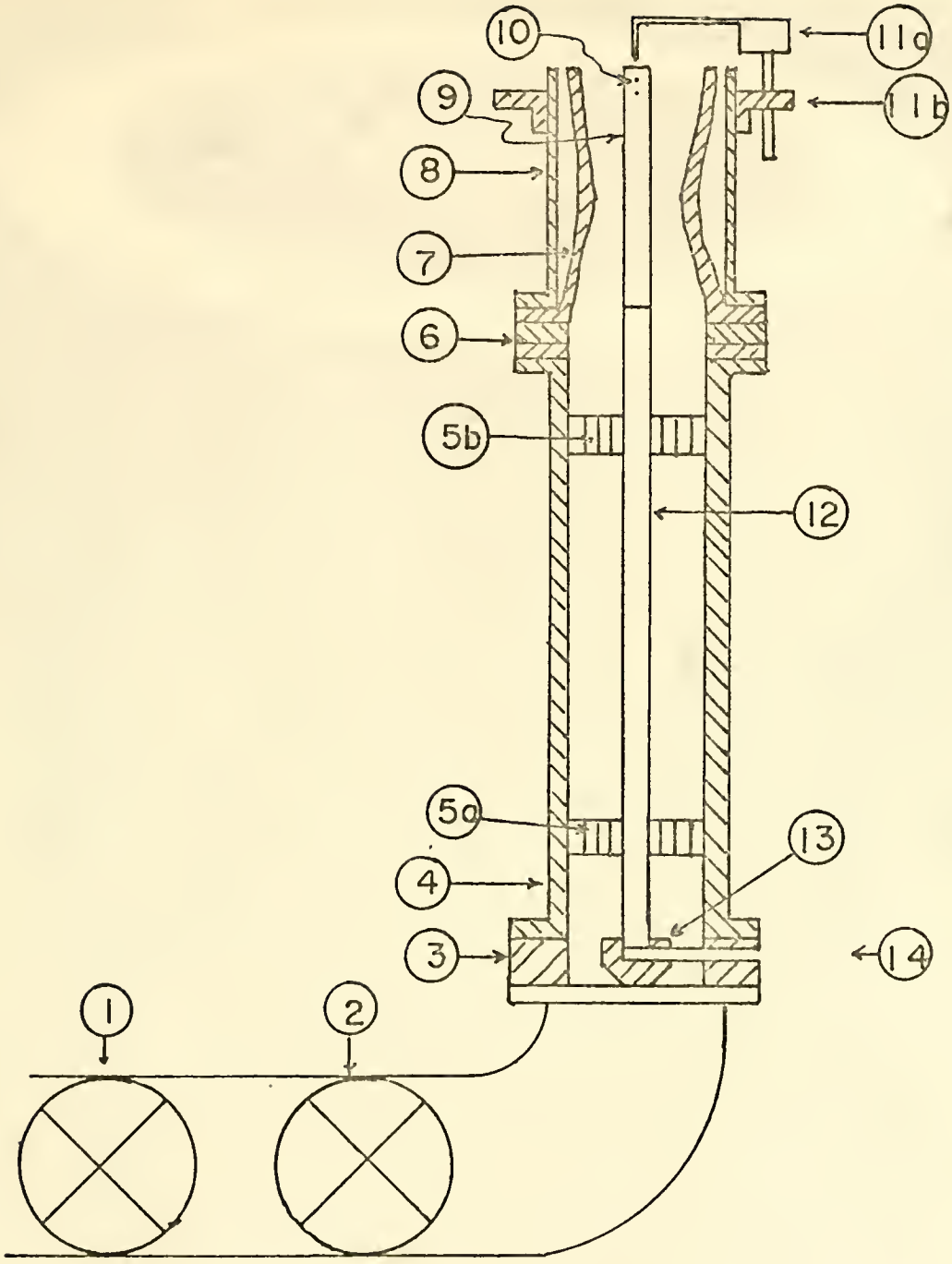

(b) Schematic
(1) Gate Valve, (2) Pressure Regulating Valve, (3) Spacer (4) Flow Straightener Section, (5a,b) Flow Straighteners, (6) Spacers for Varying P/r, (7) Epoxy Nozzle, (8) Armor Plate, (9) Cylinder, (10) Static Pressure Taps, (11a) Pitot-Static Probe, (11b) Pitot-Static Probe Support, (12) Cylinder Extension, (13) Cap-Tube Assembly, (14) Exit for Plastic Tubing for Pressure Taps

Figure 8. (Continued) Free Jet Wind Tunnel.

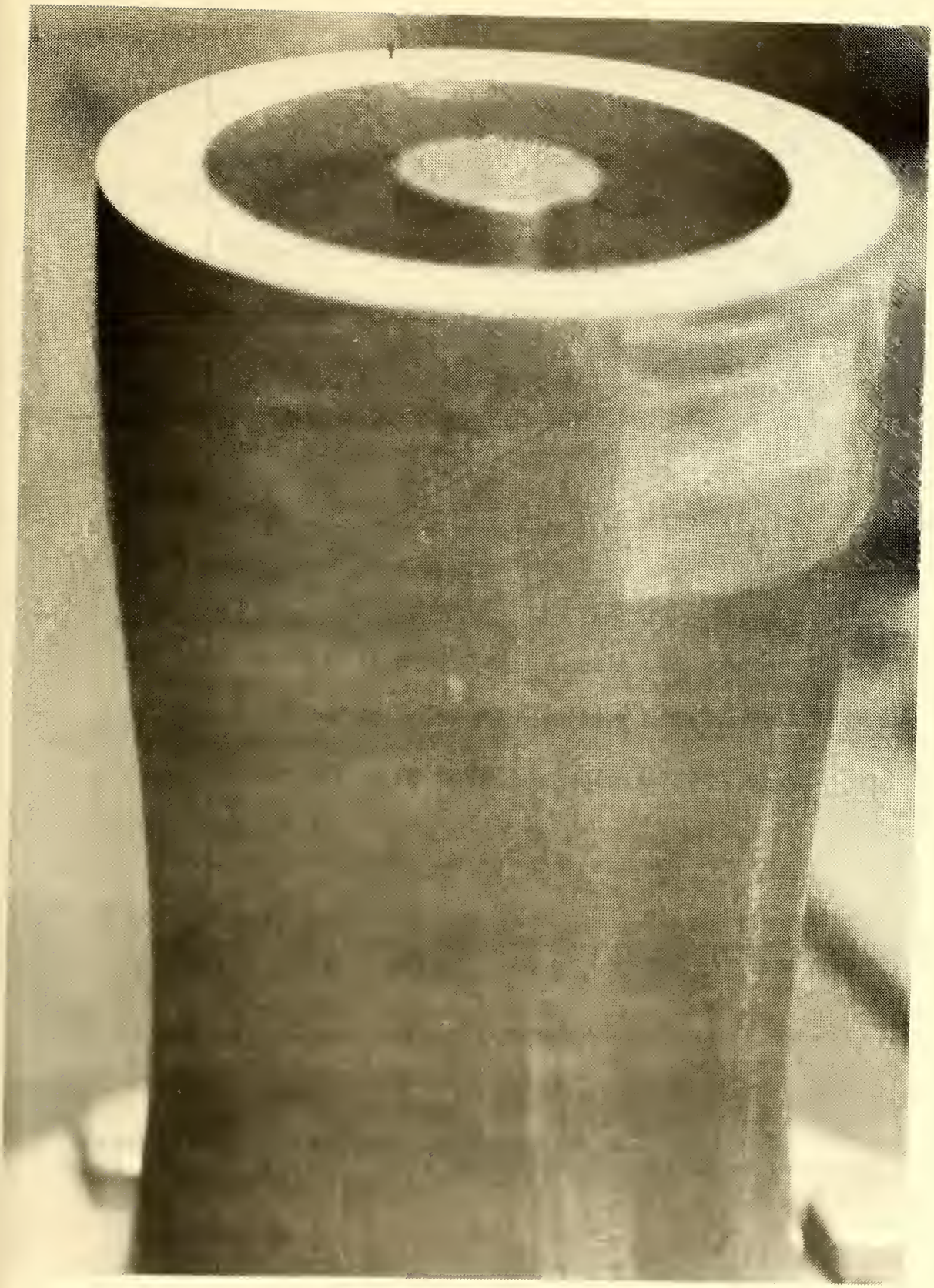

Figure 9. Photograph of Nozzle and Cylinder.

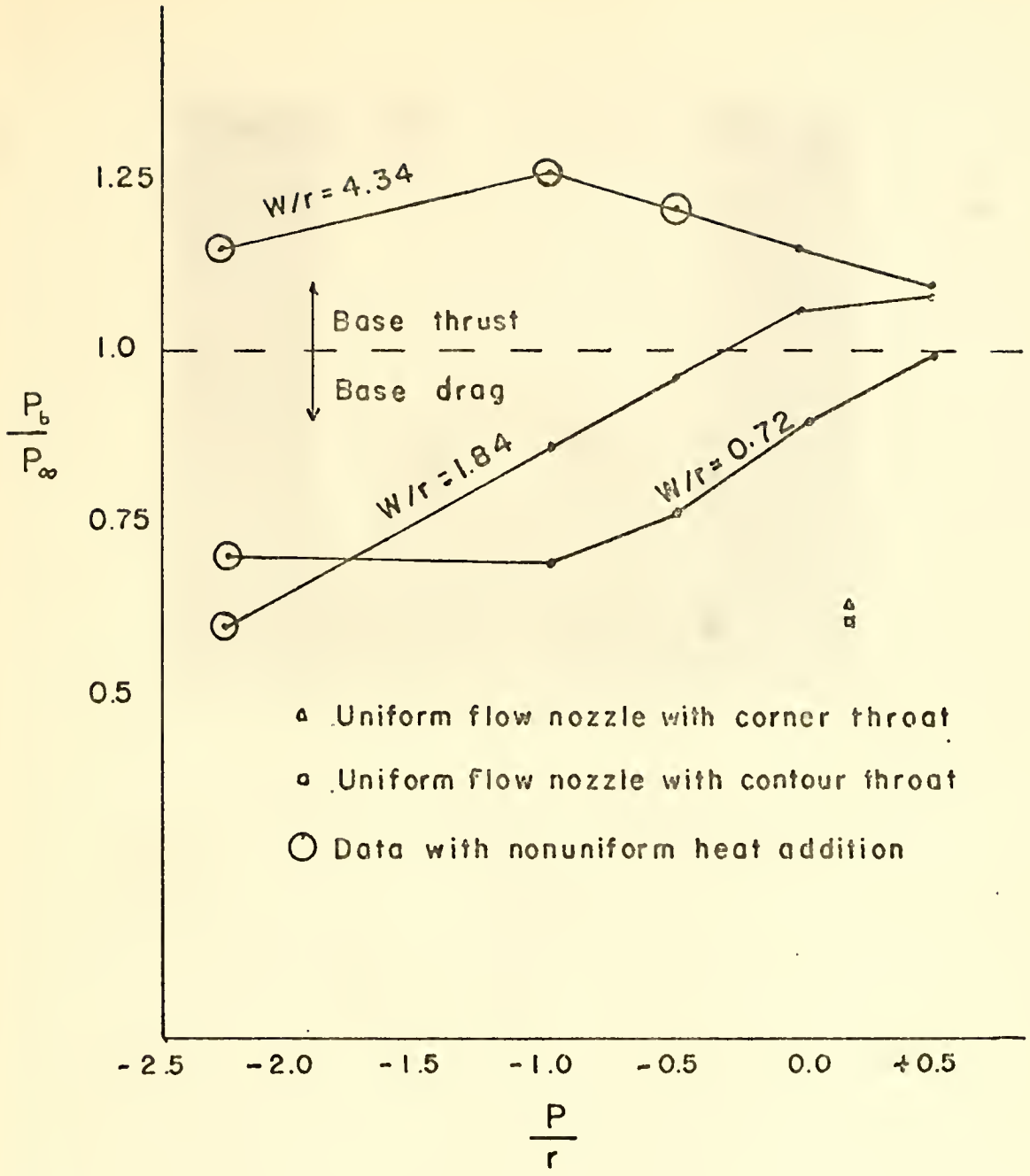

Figure 10. Base Pressure Ratio as a Function of the Position of Initial Heat Addition for a Given Length.

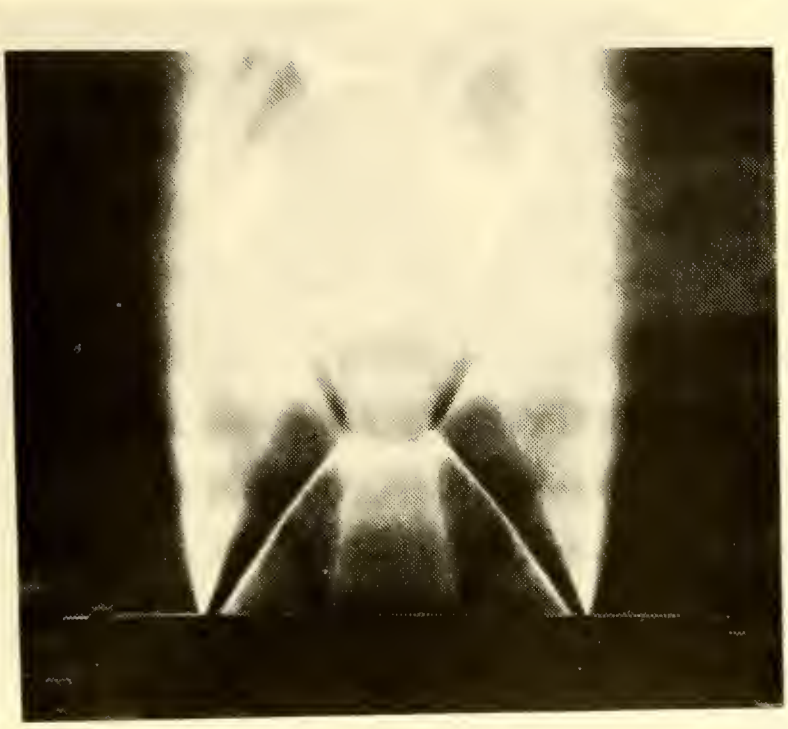

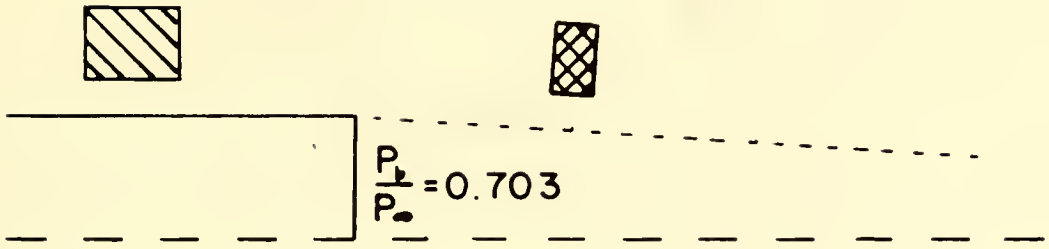

Figure 11. Photograph of the Flow for W/r = 0.72 at P/r = −2.23 and Drawing Representing Location and Extent of Heat Addition.

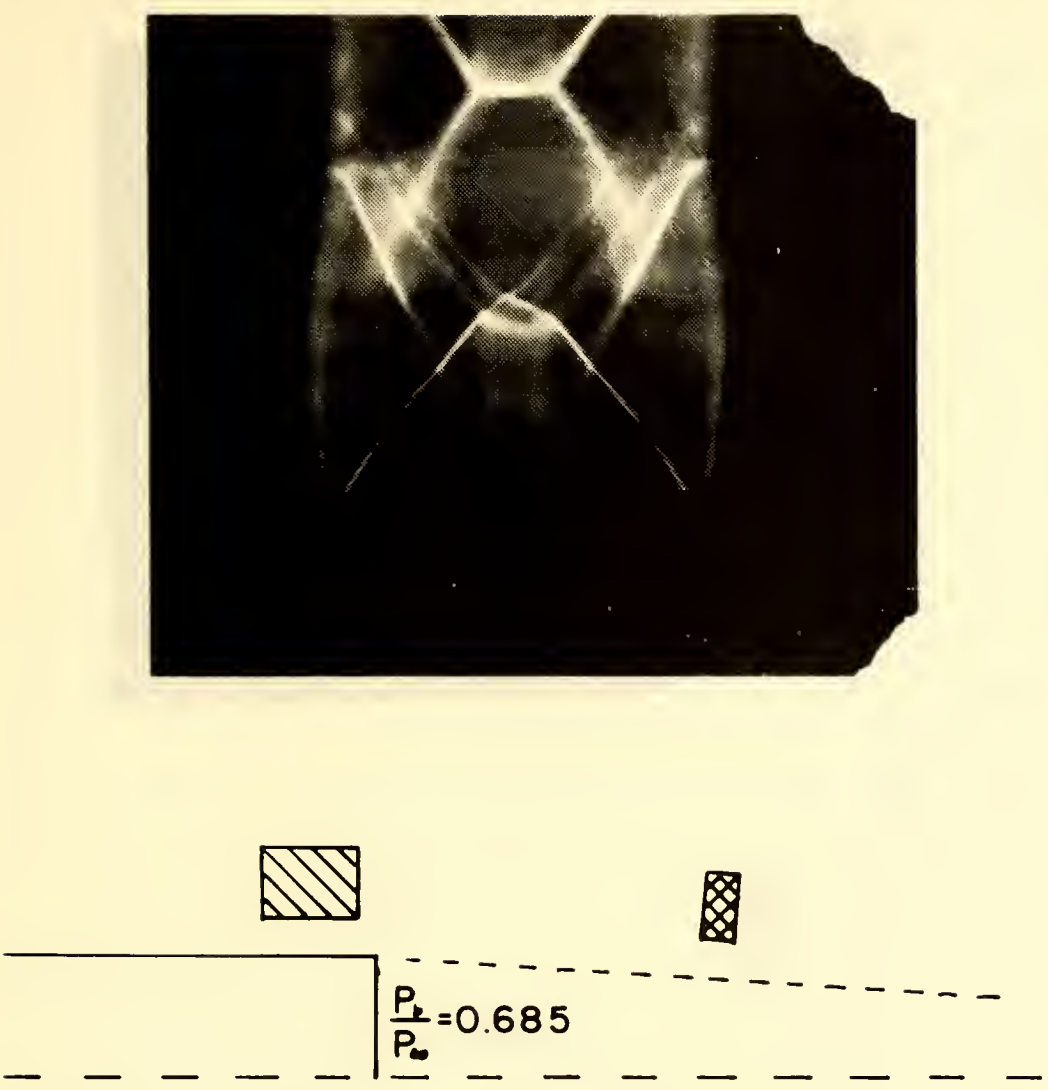

Figure 12. Photograph of the Flow for W/r = 0.72 at P/r = −0.95 and Drawing Representing Location and Extent of Heat Addition.

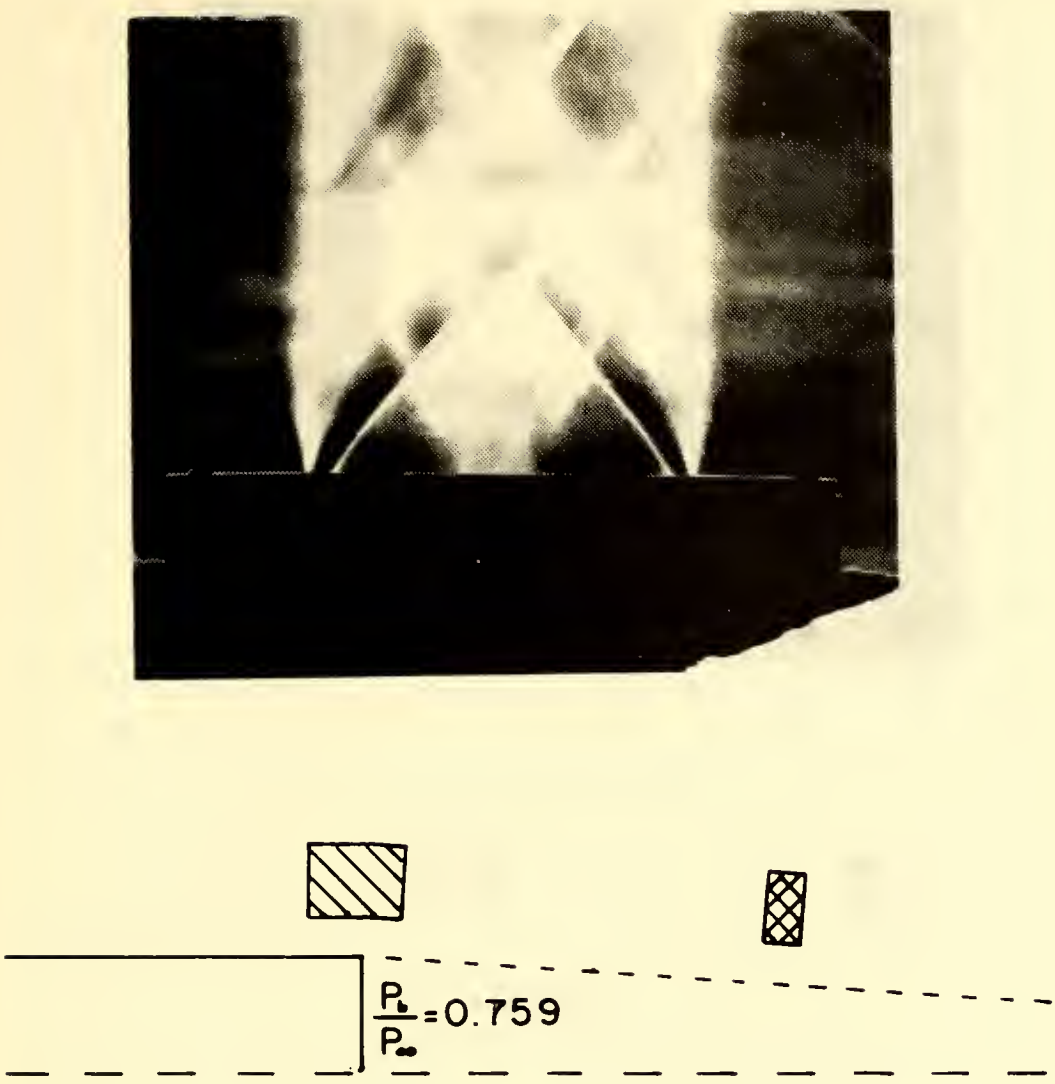

Figure 13. Photograph of the Flow for W/r = 0.72 at P/r = −0.5 and Drawing Representing Location and Extent of Heat Addition.

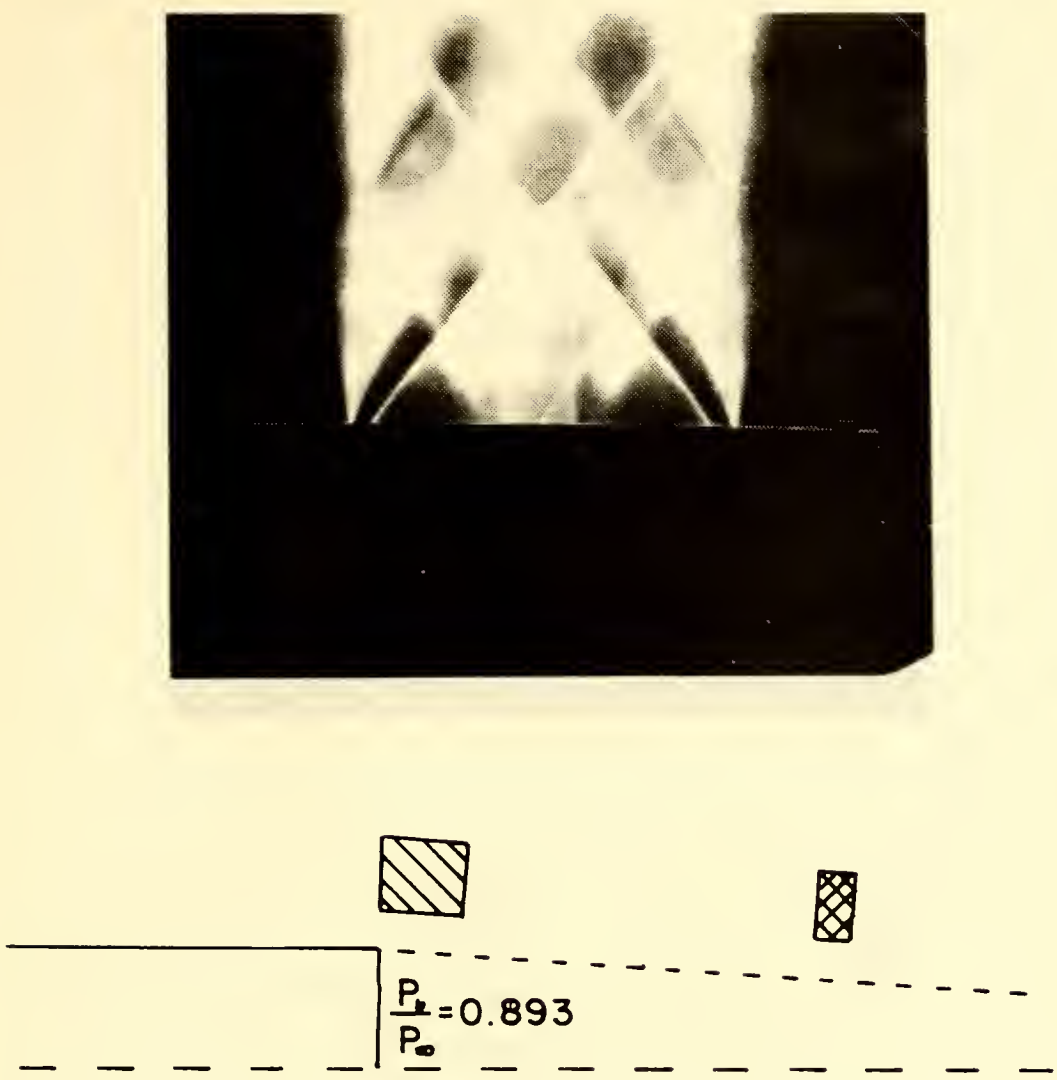

Figure 14. Photograph of the Flow for W/r = 0.72 at P/r = 0.0 and Drawing Representing Location and Extent of Heat Addition.

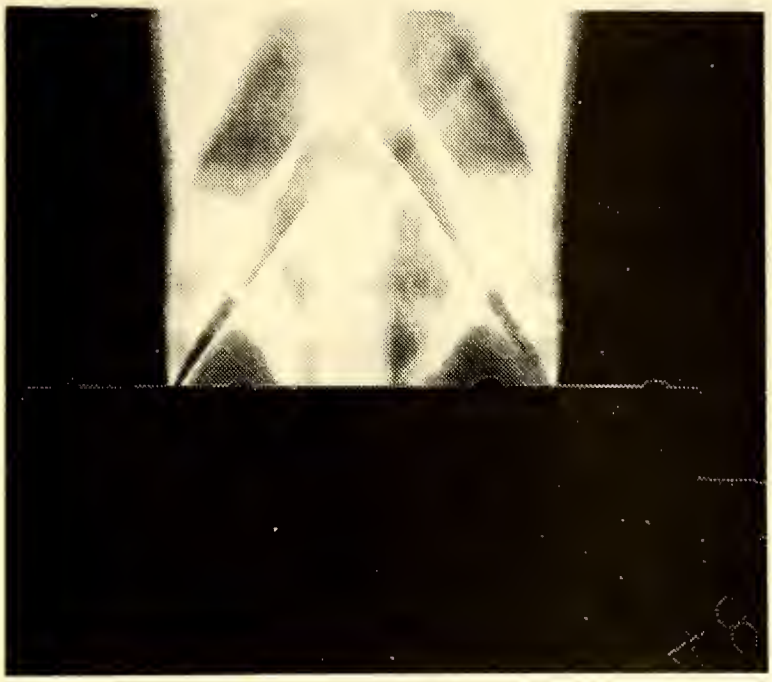

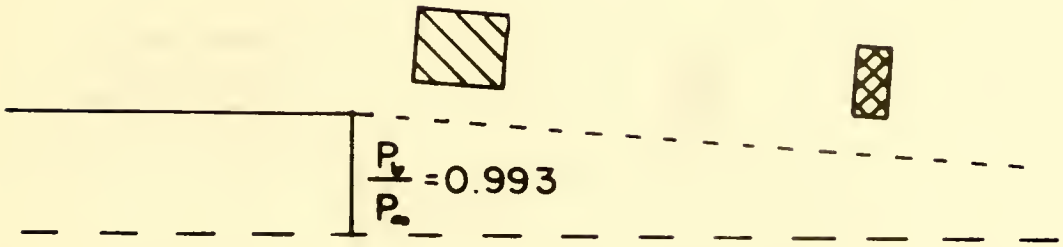

Figure 15. Photograph of the Flow for W/r = 0.72 at P/r = 0.5 and Drawing Representing Location and Extent of Heat Addition.

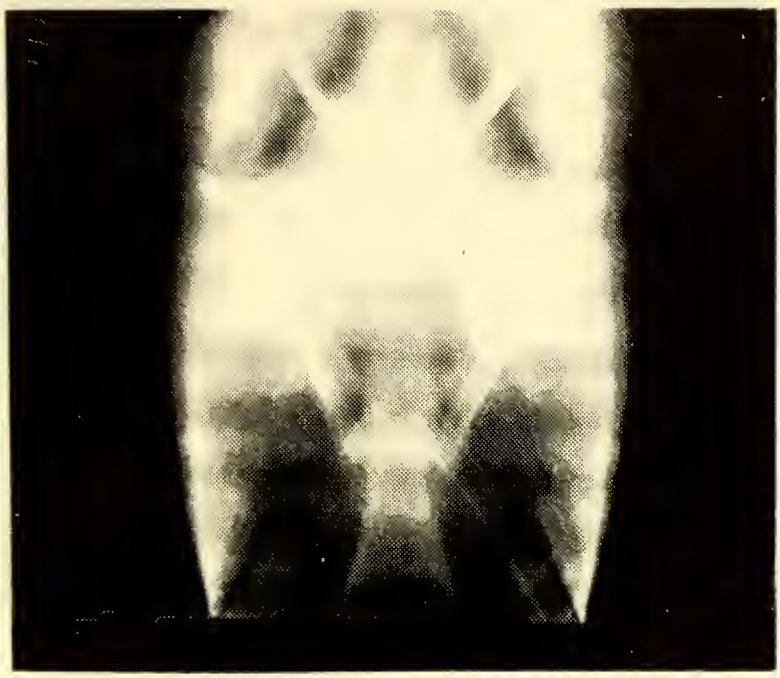

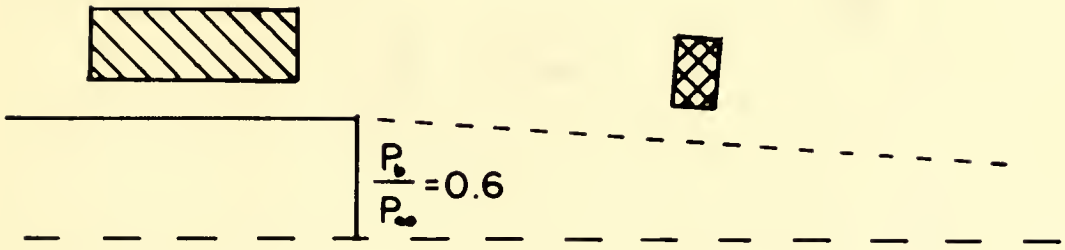

Figure 16. Photograph of the Flow for W/r = 1.84 at P/r = −2.23 and Drawing Representing Location and Extent of Heat Addition.

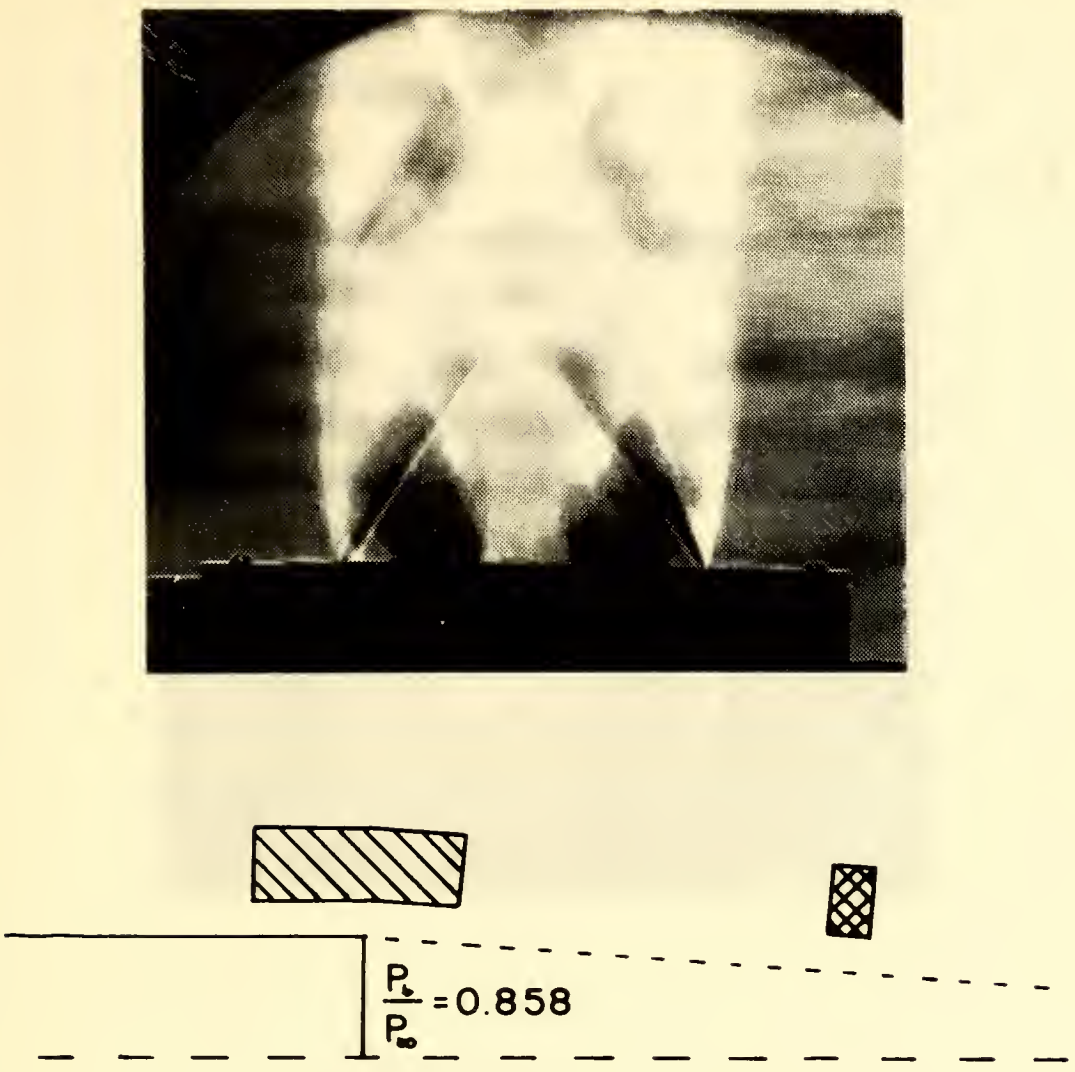

Figure 17. Photograph of the Flow for W/r = 1.84 at P/r = −0.95 and Drawing Representing Location and Extent of Heat Addition.

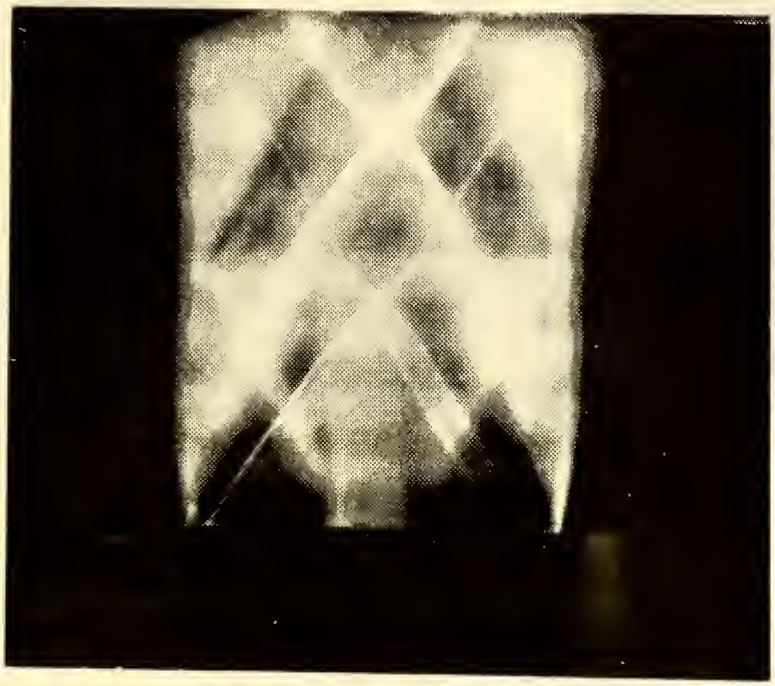

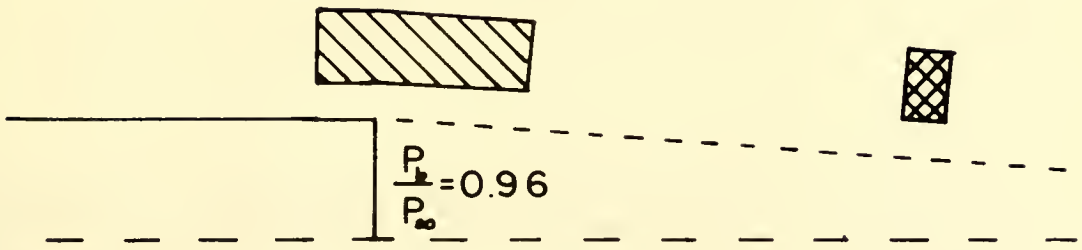

Figure 18. Photograph of the Flow for W/r = 1.84 at P/r = −0.5 and Drawing Representing Location and Extent of Heat Addition.

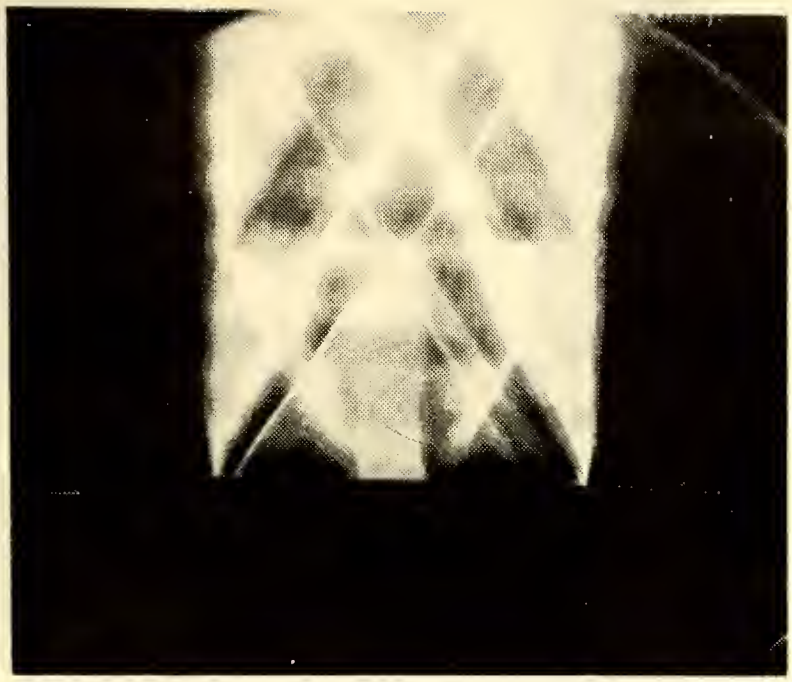

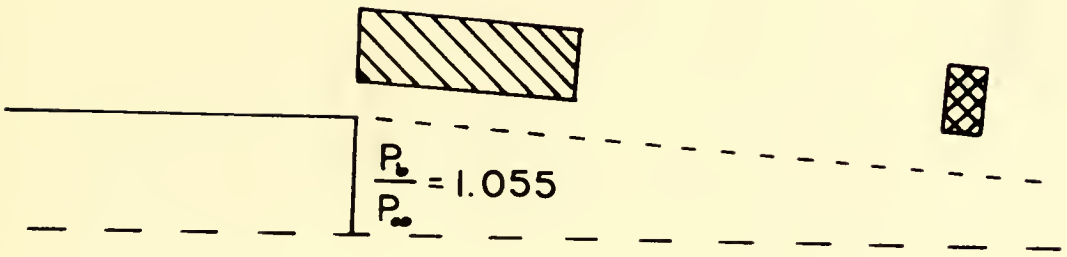

Figure 19. Photograph of the Flow for W/r = 1.84 at P/r = 0.0 and Drawing Representing Location and Extent of Heat Addition.

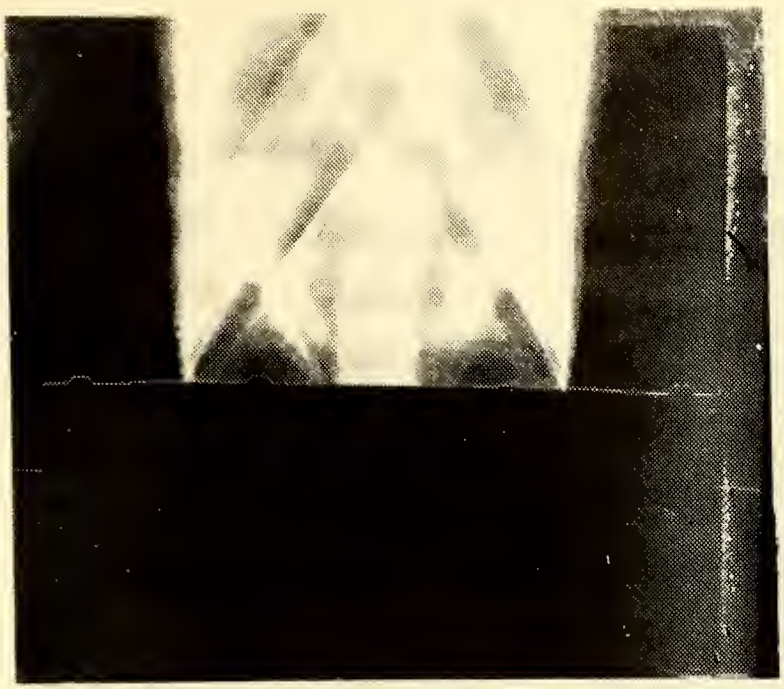

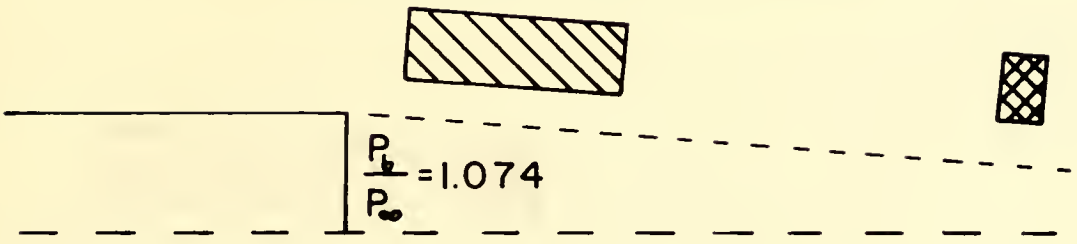

Figure 20. Photograph of the Flow for W/r = 1.84 at P/r = 0.5 and Drawing Representing Location and Extent of Heat Addition.

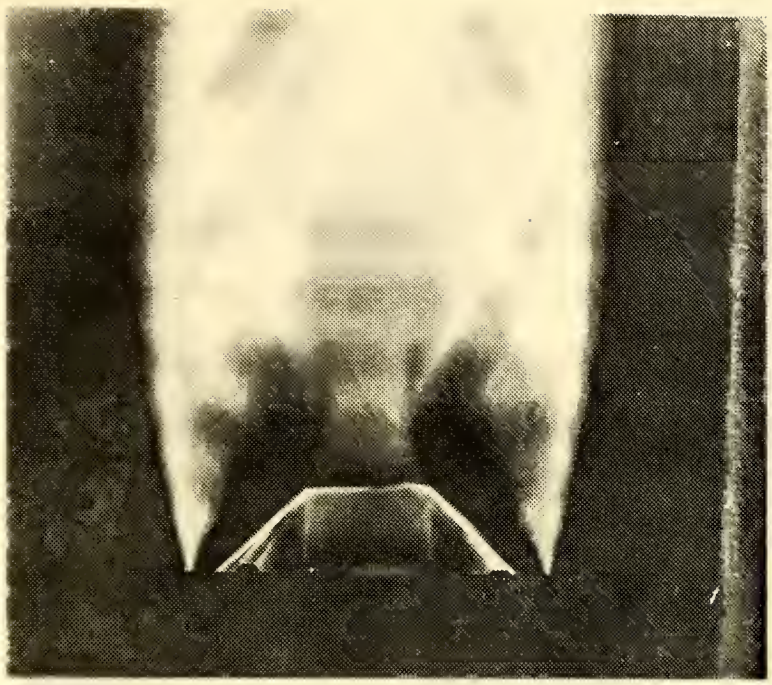

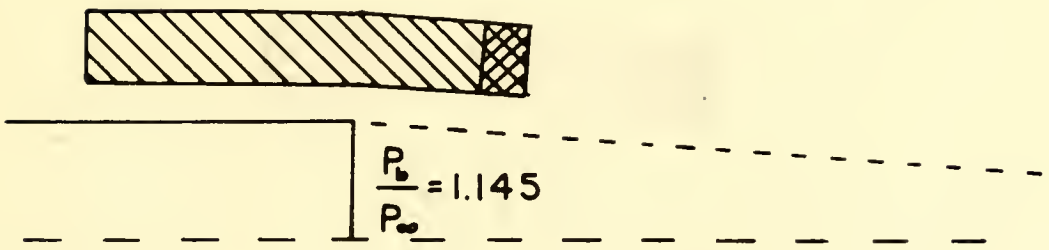

Figure 21. Photograph of the Flow for W/r = 4.34 at P/r = −2.23 and Drawing Representing Location and Extent of Heat Addition.

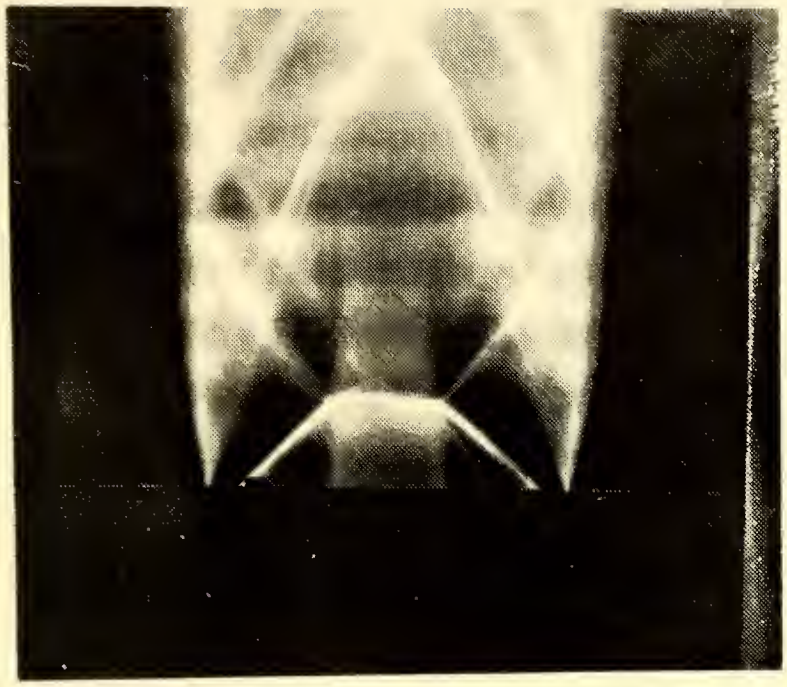

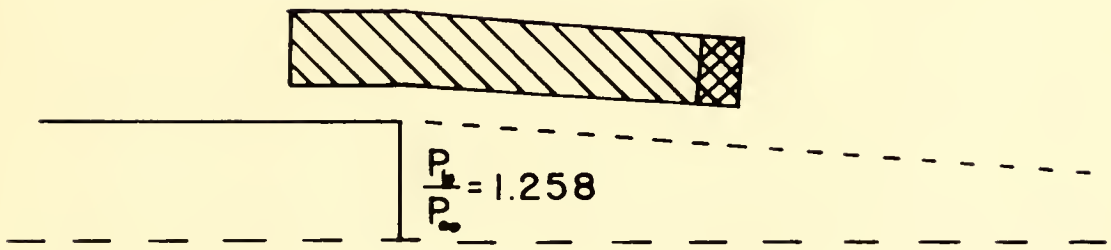

Figure 22. Photograph of the Flow for W/r = 4.34 at P/r = −0.95 and Drawing Representing Location and Extent of Heat Addition.

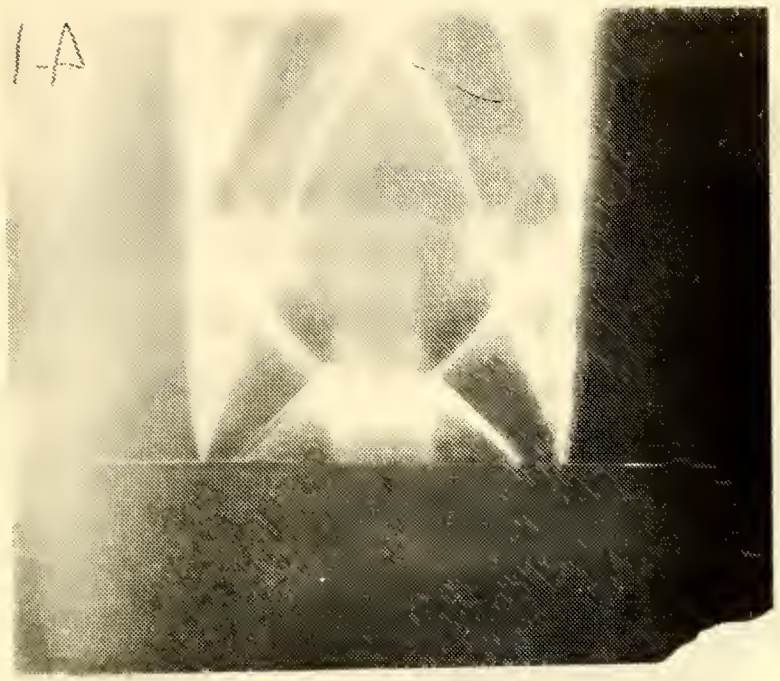

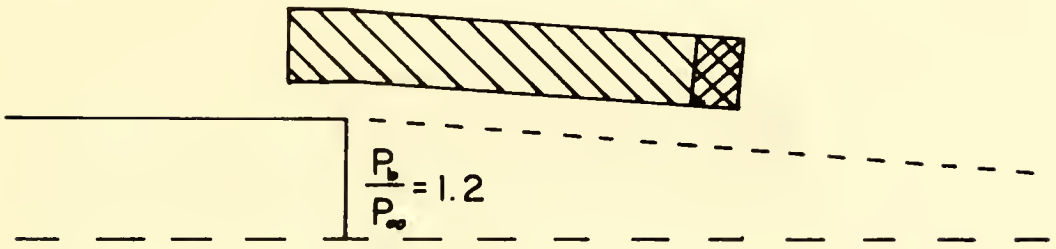

Figure 23. Photograph of the Flow for W/r = 4.34 at P/r = −0.5 and Drawing Representing Location and Extent of Heat Addition.

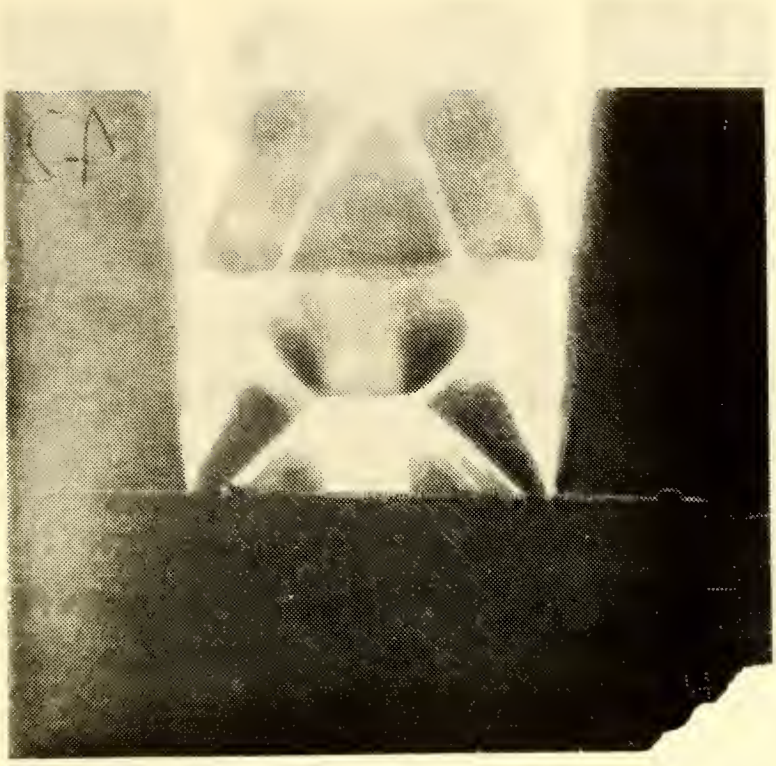

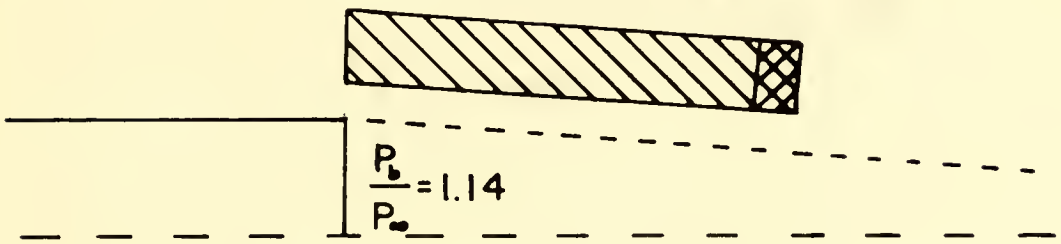

Figure 24. Photograph of the Flow for W/r = 4.34 at P/r = 0.0 and Drawing Representing Location and Extent of Heat Addition.

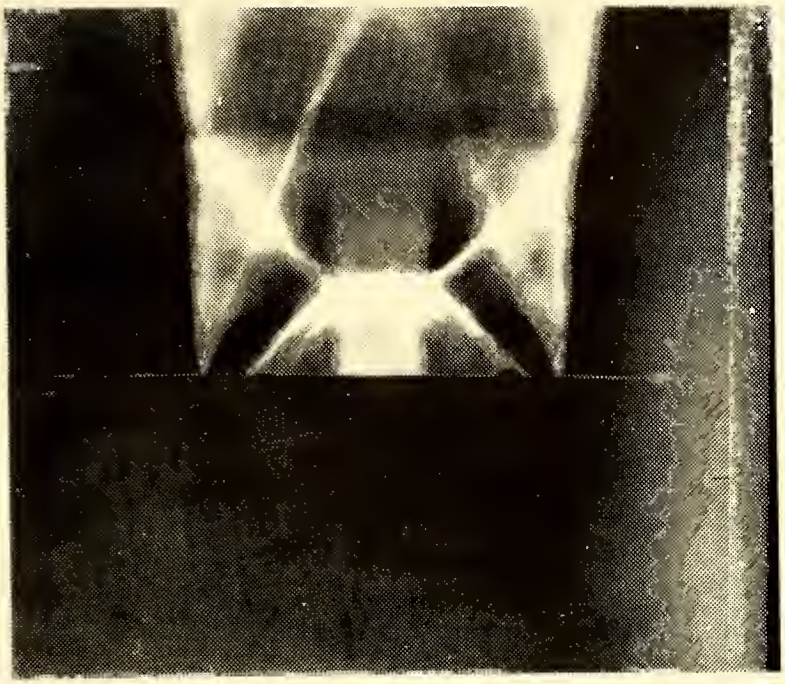

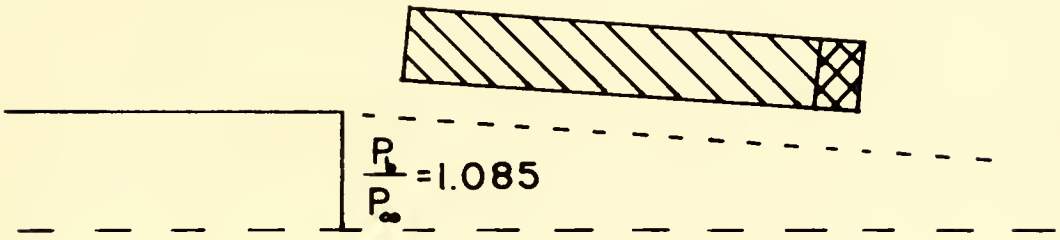

Figure 25. Photograph of the Flow for W/r = 4.34 at P/r = 0.5 and Drawing Representing Location and Extent of Heat Addition.

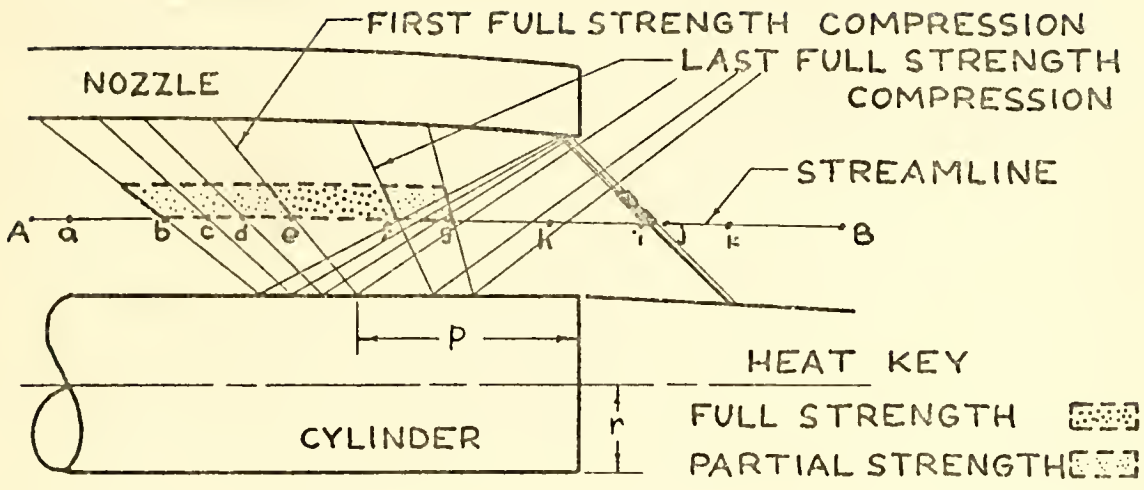

Figure 26. Results of Analysis of Reflected Waves for W/r = 0.72 (Reproduced from the MSAE Thesis of LTJG G. Caswell).

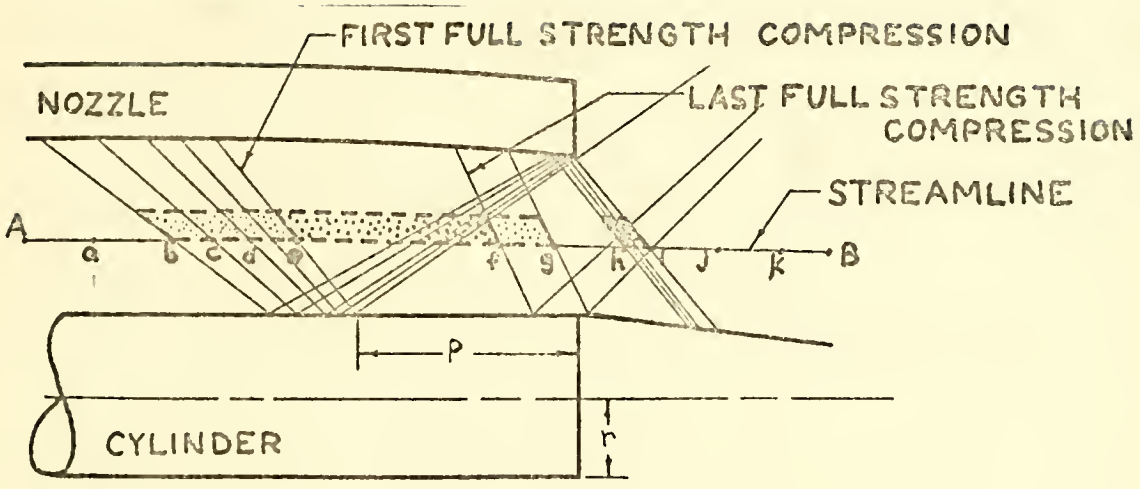

Figure 27. Results of Analysis of Reflected Waves for W/r = 1.84 (Reproduced from the MSAE Thesis of LTJG G. Caswell).

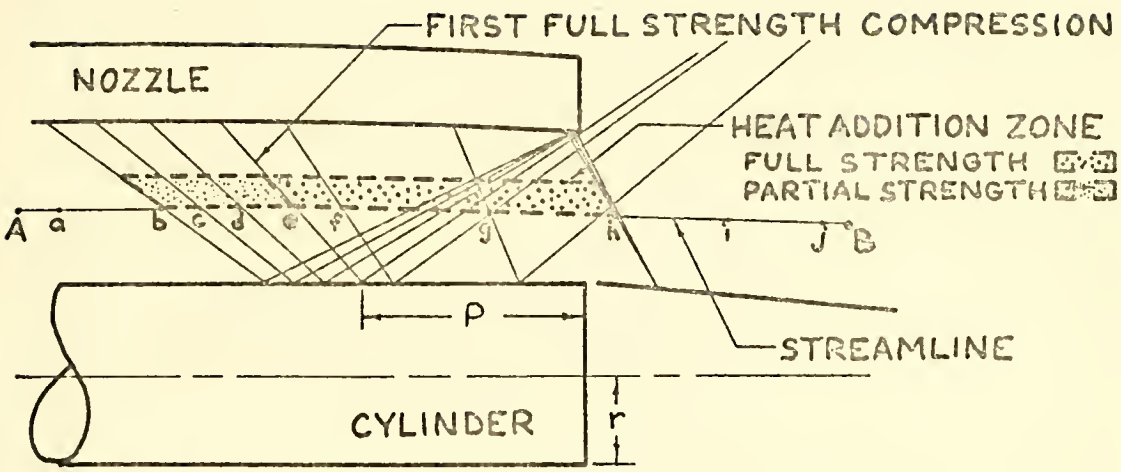

Figure 28. Results of Analysis of Reflected Waves for W/r = 4.34 (Reproduced from the MSAE Thesis of LTJG G. Caswell).

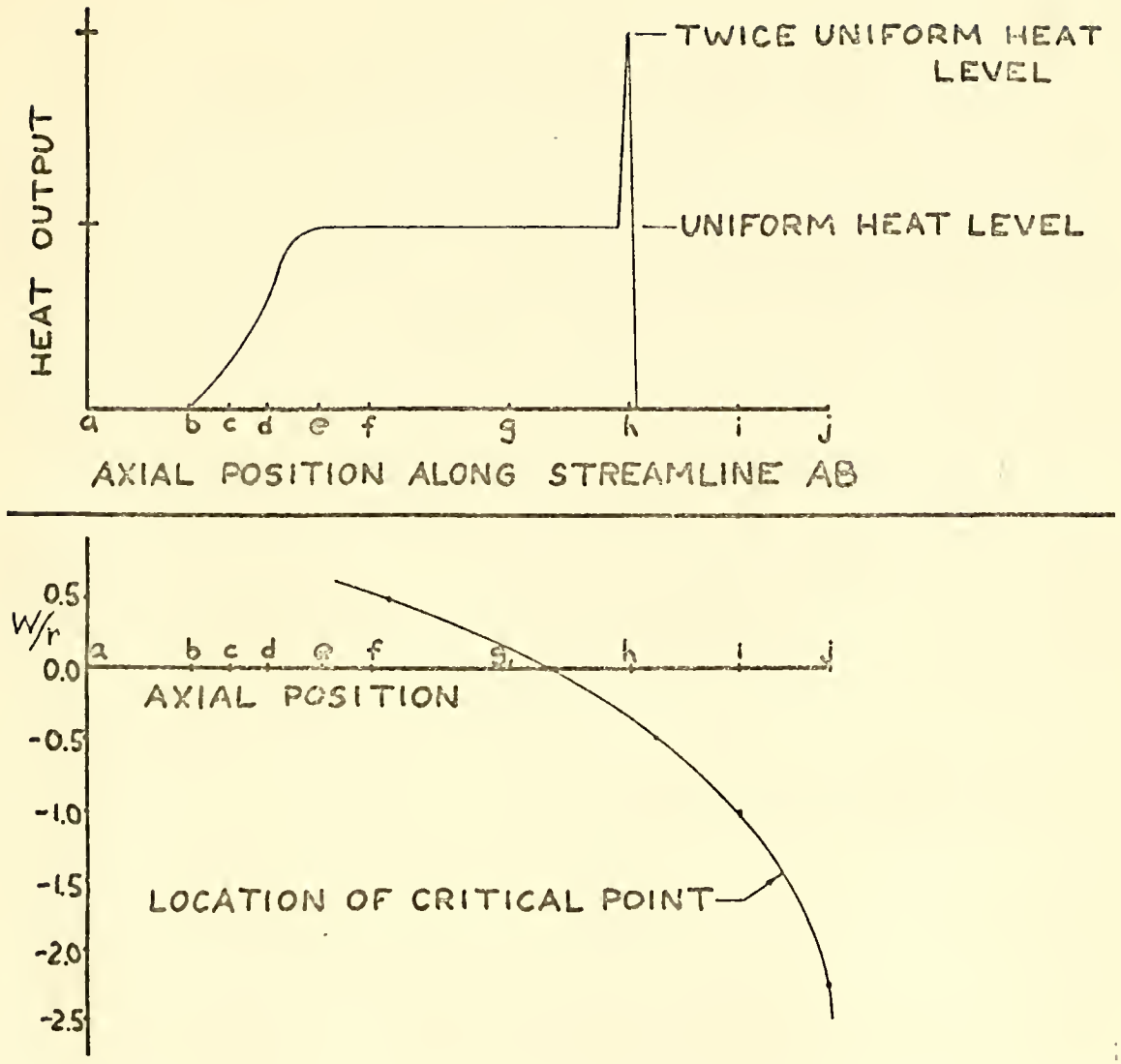

Figure 29. Distribution of Simulated Heat Addition as a Function of Axial Position Correlated to the Base Flow Sonic Line for W/r = 4.34
(Reproduced from the MSAE Thesis of LTJG Caswell).

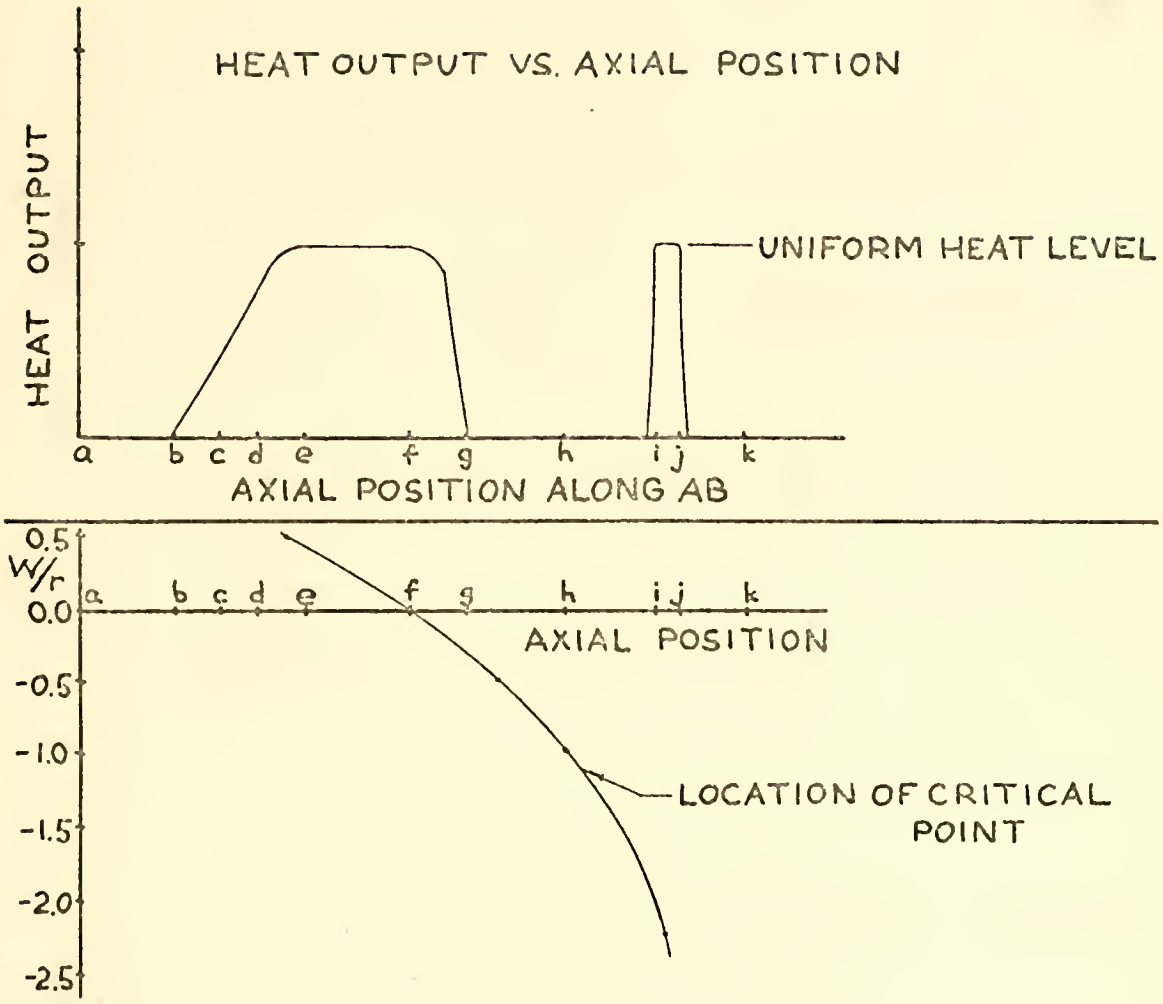

Figure 30. Distribution of Simulated Heat Addition as a Function of Axial Position Correlated to the Base Flow Sonic Line for W/r = 0.72.
(Reproduced from the MSAE Thesis of LTJG G. Caswell).

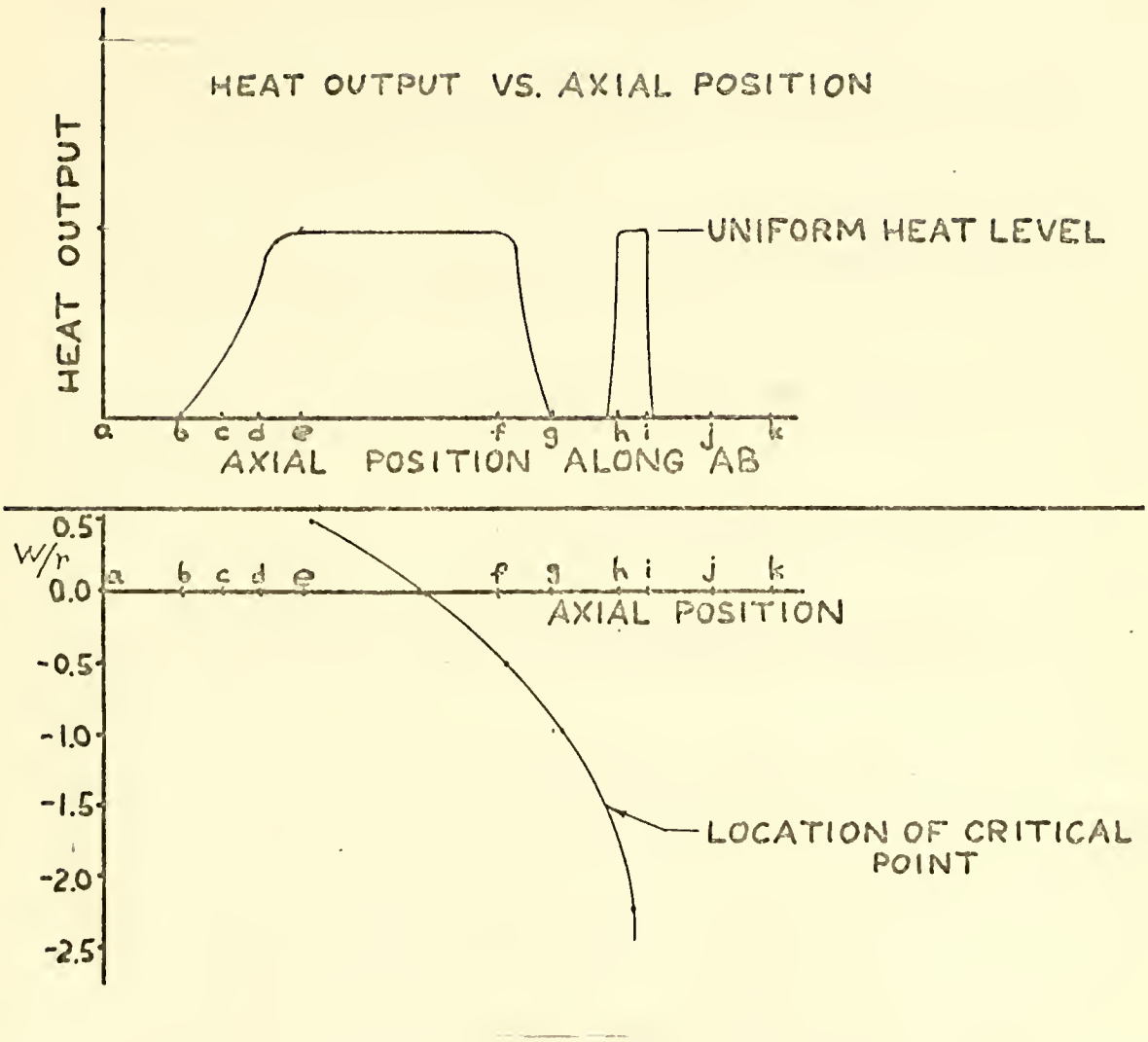

Figure 31. Distribution of Simulated Heat Addition as a Function of the Axial Position Correlated to the Base Flow Sonic Line for W/r = 1.84
(Reproduced from the MSAE Thesis of LTJG G. Caswell).

BIBLIOGRAPHY

1. Crocco, Luigi and Lees, Lester, "A Mixing Theory for the Interaction Between Dissipative Flows and Nearly Isentropic Streams," Journal of the Aeronautical Sciences, Vol. 19, No. 10, pp. 649–676, Oct. 1952.

2. Strahle, Warren C., Theoretical Consideration of Combustion Effects on Base Pressure in Supersonic Flight, Twelfth Symposium on Combustion Institute, Pittsburgh, Pa., pp. 1163–1173, 1969.

3. Davis, D. D., Extension of Simplified Mixing Theory to Axially Symmetric Supersonic Wake Flows and Application to Base Pressure Problem for a Body of Revolution, M.Sc. Thesis, Princeton University, 1952.

4. Stewartson, K., The Theory of Laminar Boundary Layers in Compressible Fluids, Oxford University Press, Oxford, 1964.

5. Owczarek, Jerzy A., Fundamentals of Gas Dynamics, International Textbook Co., Scranton, Pa., June, 1968.

6. de Kransinski, Joseph S. A., A Study of Axially Symmetrical Base Flow Behind Bodies of Revolution at Supersonic Speeds, Ph.D. Thesis, London University, 1964.

7. Fuhs, A. E., Quasi Area Rule for Heat Addition in Transonic and Supersonic Flight Regimes, Technical Report, AFAPL-TR-72-10, Aug. 1972.

8. Smithey, William and Naber, Michael, "Sonic Line Shape for a Coaxial Nozzle Geometry," AIAA Journal, Vol. 11, No. 4, pp. 569, Apr. 1973.

9. Przirembel, C. E. G. and Page, R. H., "Analysis of Axisymmetric Supersonic Turbulent Base Flow," Heat Transfer and Fluid Mechanics Institute Proceedings, pp. 258–272, 1968.

INITIAL DISTRIBUTION LIST

		No. Copies
1.	Defense Documentation Center Cameron Station Alexandria, Virginia 22314	2
2.	Library, Code 0212 Naval Postgraduate School Monterey, California 93940	2
3.	Chairman, Department of Aeronautics Naval Postgraduate School Monterey, California 93940	2
4.	Professor A. Fuhs Code 57 Department of Aeronautics Naval Postgraduate School Monterey, California 93940	5
5.	Lieutenant M. E. Naber USN Rt 1, Box 1048 Sequim, Washington 98382	1
6.	Commander W. Smithey Department of Aeronautics Naval Postgraduate School Monterey, California 93940	1
7.	Dr. Warren Strahle Associate Professor Georgia Institute of Technology Atlanta, Georgia 30332	1
8.	Dominic J. Monetta Gun System Engineering Naval Ordnance Station Indian Head, Maryland 20640	2
9.	Alan Roberts Gun System Engineering Naval Ordnance Station Indian Head, Maryland 20640	2
10.	Dr. Frederick Billig Applied Physics Lab. John Hopkins University 8621 Georgia Avenue Silver Spring, Maryland 20910	1

11. Professor Bruce Reese — 1
Purdue University
Lafayette, Indiana 47907

12. Dr. James S. Holdhausen — 1
Vice President, FluiDyne Engr. Corp.
5900 Olsen Hwy
Minneapolis, Minnesota 55422

13. Tom Curran — 1
Chief, Ramjet Technology Branch
AFADL
WPAFB, Ohio 45433

14. Grant Hosack — 1
RocketDyne
Rockwell International
6633 Canoga Avenue
Canoga Park, California 91304

15. C. C. Miner — 1
U. S. Army Missile Command
Redstone Arsenal, Alabama 35808

16. Dr. Richard Weiss — 1
AF Rocket Propulsion Lab.
Edwards AFB, California 93523

17. Dr. Ing. G. Winterfeld — 1
D F V L R
Institut f. Luftstrahlantriebe
505 Porz-Wahn, Linder Höhe, Germany

SECURITY CLASSIFICATION OF THIS PAGE (When Data Entered)

REPORT DOCUMENTATION PAGE		READ INSTRUCTIONS BEFORE COMPLETING FORM
1. REPORT NUMBER	2. GOVT ACCESSION NO.	3. RECIPIENT'S CATALOG NUMBER
4. TITLE (and Subtitle) Investigation of External Burning Assisted Projectile		5. TYPE OF REPORT & PERIOD COVERED Master's Thesis September 1973 6. PERFORMING ORG. REPORT NUMBER
7. AUTHOR(s) Michael Edmund Naber		8. CONTRACT OR GRANT NUMBER(s)
9. PERFORMING ORGANIZATION NAME AND ADDRESS Naval Postgraduate School Monterey, California 93940		10. PROGRAM ELEMENT, PROJECT, TASK AREA & WORK UNIT NUMBERS
11. CONTROLLING OFFICE NAME AND ADDRESS Naval Postgraduate School Monterey, California 93940		12. REPORT DATE September 1973 13. NUMBER OF PAGES 72
14. MONITORING AGENCY NAME & ADDRESS(If different from Controlling Office) Naval Postgraduate School Monterey, California 93940		15. SECURITY CLASS. (of this report) Unclassified 15a. DECLASSIFICATION/DOWNGRADING SCHEDULE

16. DISTRIBUTION STATEMENT (of this Report)

Approved for public release; distribution unlimited.

17. DISTRIBUTION STATEMENT (of the abstract entered in Block 20, if different from Report)

18. SUPPLEMENTARY NOTES

19. KEY WORDS (Continue on reverse side if necessary and identify by block number)

20. ABSTRACT (Continue on reverse side if necessary and identify by block number)

External burning reduces the base drag of a supersonic projectile by increasing the base pressure. Drag reduction is of interest due to the increase in range, decreased time of flight, and/or increased impact velocity. Theoretically, the Crocco-Lees analytical model for base flow is reviewed for axisymmetric flow without heat addition and for planar flow with heat addition. A free jet wind facility

DD FORM 1 JAN 73 1473 EDITION OF 1 NOV 65 IS OBSOLETE
S/N 0102-014-6601 |
(Page 1)

SECURITY CLASSIFICATION OF THIS PAGE (When Data Entered)

has been constructed for simulation of a projectile with heat addition. Heat addition is found to give base thrust and, therefore, provides a method for increasing the performance of a gun system.

Thesis
N15
c.1
146325
Naber
Investigation of external burning assisted projectile.